**Atmospheric
Chemistry
and Physics**

Cloud condensation nuclei in polluted air and biomass burning smoke near the mega-city Guangzhou, China – Part 1: Size-resolved measurements and implications for the modeling of aerosol particle hygroscopicity and CCN activity

D. Rose[1], **A. Nowak**[2], **P. Achtert**[2], **A. Wiedensohler**[2], **M. Hu**[3], **M. Shao**[3], **Y. Zhang**[3], **M. O. Andreae**[1], **and U. Pöschl**[1]

[1]Biogeochemistry Department, Max Planck Institute for Chemistry, Mainz, Germany
[2]Leibniz Institute for Tropospheric Research, Leipzig, Germany
[3]State Key Joint Laboratory of Environmental Simulation and Pollution Control, College of Environmental Sciences and Engineering, Peking University, Beijing, China

Abstract. Atmospheric aerosol particles serving as Cloud Condensation Nuclei (CCN) are key elements of the hydrological cycle and climate. We measured and characterized CCN in polluted air and biomass burning smoke during the PRIDE-PRD2006 campaign from 1–30 July 2006 at a rural site $\sim$60 km northwest of the mega-city Guangzhou in southeastern China.

CCN efficiency spectra (activated fraction vs. dry particle diameter; 20–290 nm) were recorded at water vapor supersaturations (S) in the range of 0.068% to 1.27%. The corresponding effective hygroscopicity parameters describing the influence of particle composition on CCN activity were in the range of $\kappa \approx$ 0.1–0.5. The campaign average value of κ=0.3 equals the average value of κ for other continental locations. During a strong local biomass burning event, the average value of κ dropped to 0.2, which can be considered as characteristic for freshly emitted smoke from the burning of agricultural waste. At low S ($\leq$0.27%), the maximum activated fraction remained generally well below one, indicating substantial portions of externally mixed CCN-inactive particles with much lower hygroscopicity – most likely soot particles (up to $\sim$60% at $\sim$250 nm).

The mean CCN number concentrations ($N_{CCN,S}$) ranged from 1000 cm^{-3} at S=0.068% to 16 000 cm^{-3} at S=1.27%, which is about two orders of magnitude higher than in pristine air. Nevertheless, the ratios between CCN concentration and total aerosol particle concentration (integral CCN efficiencies) were similar to the ratios observed in pristine continental air ($\sim$6% to $\sim$85% at S=0.068% to 1.27%). Based on the measurement data, we have tested different model approaches for the approximation/prediction of $N_{CCN,S}$. Depending on S and on the model approach, the relative deviations between observed and predicted $N_{CCN,S}$ ranged from a few percent to several hundred percent. The largest deviations occurred at low S with a simple power law. With a Köhler model using variable κ values obtained from individual CCN efficiency spectra, the relative deviations were on average less than $\sim$10% and hardly exceeded 20%, confirming the applicability of the κ-Köhler model approach for efficient description of the CCN activity of atmospheric aerosols. Note, however, that different types of κ-parameters must be distinguished for external mixtures of CCN-active and -inactive aerosol particles (κ_a, κ_t, κ_{cut}). Using a constant average hygroscopicity parameter (κ=0.3) and variable size distributions as measured, the deviations between observed and predicted CCN concentrations were on average less than 20%. In contrast, model calculations using variable hygroscopicity parameters as measured and constant size distributions led to much higher deviations: $\sim$70% for the campaign average size distribution, $\sim$80% for a generic rural size distribution, and $\sim$140% for a generic urban size distribution. These findings confirm earlier studies suggesting that aerosol particle number and size are the major predictors for the

---

Correspondence to: D. Rose
(d.rose@mpic.de)

variability of the CCN concentration in continental boundary layer air, followed by particle composition and hygroscopicity as relatively minor modulators. Depending on the required and applicable level of detail, the information and parameterizations presented in this study should enable efficient description of the CCN activity of atmospheric aerosols in detailed process models as well as in large-scale atmospheric and climate models.

1 Introduction

Atmospheric aerosol particles that enable the condensation of water vapor and formation of cloud droplets are called Cloud Condensation Nuclei (CCN). Elevated concentrations of CCN tend to increase the concentration and decrease the size of droplets in a cloud. Besides changing the optical properties and the radiative effects of clouds on climate, this may lead to the suppression of precipitation in shallow and short-lived clouds and to greater convective overturning and more precipitation in deep convective clouds (Rosenfeld et al., 2008). The response of cloud characteristics and precipitation processes to increasing anthropogenic aerosol concentrations represents one of the largest uncertainties in the current understanding of climate change. One of the crucial underlying challenges is to determine the ability of aerosol particles to act as CCN under relevant atmospheric conditions, an issue that has received increasing attention over the past years (McFiggans et al., 2006; IAPSAG, 2007; IPCC, 2007; Andreae and Rosenfeld, 2008, and references therein).

In order to incorporate the effects of CCN in meteorological models at all scales, from Large Eddy Simulation (LES) to Global Climate Models (GCM), knowledge of the spatial and temporal distribution of CCN in the atmosphere is essential (Huang et al., 2007). In recent years, anthropogenic emissions of aerosol particles and precursors from Asia have increased significantly (Streets et al., 2000, 2008; Richter et al., 2005; Shao et al., 2006), and numerous studies indicate that anthropogenic aerosol particles have changed cloud microphysical and radiative properties (Xu, 2001; Liu et al., 2004; Massie et al., 2004; Zhang et al., 2004; Wang et al., 2005; Qian et al., 2006; Zhao et al., 2006; Li et al., 2007; Rosenfeld et al., 2007; Deng et al., 2008). Thus, CCN data are required for assessing the impact of anthropogenic aerosol on regional and global climate. Several earlier and recent studies have reported CCN measurements from various regions around the world (e.g., Andreae, 2009; Andreae and Rosenfeld, 2008; Bougiatioti et al., 2009; Broekhuizen et al., 2006; Chang et al., 2009; Dusek et al., 2006, 2010; Ervens et al., 2009; Gunthe et al., 2009; Lance et al., 2009; Pöschl et al., 2009; Roberts et al., 2001, 2002, 2006; Shantz et al., 2009; Wang et al., 2008; and references therein). However, only few CCN measurements have been performed in Asia and in the vicinity of mega-cities and city-clusters, which are major source regions of air particulate matter (e.g. Matsumoto et al., 1997; Yum et al., 2005, 2007; Kuwata et al., 2007, 2008, 2009; Wiedensohler et al., 2009).

The Pearl River Delta (PRD) in southeastern China is one of the main centers of economic activity and growth in Asia. Due to strong anthropogenic emissions, the PRD region is often plagued with high aerosol concentrations that not only lead to low visibility, but can also impact the regional radiative balance, precipitation patterns and hydrological cycles (Hagler et al., 2006; Andreae et al., 2008; Fan et al., 2008; Wendisch et al., 2008; Zhang et al., 2008).

Within the "Program of Regional Integrated Experiments of Air Quality over the Pearl River Delta" intensive campaign in July 2006 (PRIDE-PRD2006), we measured and characterized the CCN properties of aerosol particles in polluted air and biomass burning smoke near the mega-city Guangzhou as a function of particle diameter (20–290 nm) and water vapor supersaturation (0.068–1.27%). In this manuscript, we focus on the results of the size-resolved CCN measurements and on the implications for different approaches of approximating and predicting CCN number concentrations. A follow-up study will address the relationships between aerosol chemical composition and CCN activity (Rose et al., 2010a).

2 Methods

2.1 Measurement location, meteorological conditions and supporting data

The measurements were performed during the period of 1–30 July 2006 in Backgarden (23.548056° N, 113.066389° E), a small village ∼60 km northwest of Guangzhou on the outskirts of the densely populated center of the PRD. Due to the prevailing southeast monsoon circulation at this time of year, the air masses came mainly from the south/southeast, making this site a rural receptor site for the regional pollution resulting from the outflow of the city cluster around Guangzhou. The average meteorological conditions (arithmetic mean ± standard deviation) for the campaign were: 28.9±3.2 °C ambient temperature, 78.0±13.7% ambient Relative Humidity (RH), 997±4 hPa ambient pressure, 1.8±1.2 m s^{-1} local wind speed, 143±53° local wind direction. For more information about the measurement location and meteorological conditions see Garland et al. (2008).

A two-story building was used exclusively to house the measurement campaign, with most of the instruments placed in air conditioned rooms on the top floor and sample inlets mounted on the rooftop. The main aerosol inlet used in this study was equipped with a Rupprecht and Patashnick PM$_{10}$ inlet (flow rate 16.7 L min^{-1}). The sample flow passed through stainless steel tubing (1.9 cm i.d., 5.1 m length) and a diffusion dryer with silica gel/molecular sieve cartridges (alternating regeneration with dry pressurized air,

regeneration cycles 15–50 min, average RH=33±7%). After drying, the sample flow was split into separate lines. One led to the CCN measurement setup described below (0.9 cm i.d. stainless steel, ∼4 m length, flow rate 1.5 L min^{-1}); another was used for aerosol particle size distribution measurements (3–900 nm) with a Twin Differential Mobility Particle Sizer (TDMPS). The inlet, dryer and size distribution measurements were operated by the Leibniz Institute for Tropospheric Research (IfT).

Besides aerosol particle size distribution and CCN activity, on which we focus in this manuscript, a wide range of other aerosol, gas phase, and meteorological parameters were measured to characterize local and regional air pollution (Garland et al., 2008; Hua et al., 2008a; Liu et al., 2008). These will be used in a follow-up study addressing the relationships between aerosol chemical composition and CCN activity (Rose et al., 2010a).

2.2 CCN measurement and data analysis

2.2.1 Instrumentation and measurement procedure

Size-resolved CCN efficiency spectra (CCN activation curves) were measured with a Droplet Measurement Technologies continuous flow CCN counter (Roberts and Nenes, 2005; Lance et al., 2006) coupled to a Differential Mobility Analyzer (DMA; TSI 3071) and a condensation particle counter (CPC; TSI 3762; Frank et al., 2006; Rose et al., 2008).

The CCN Counter (CCNC) was operated at a total flow rate of 0.5 L min^{-1} with a sheath-to-aerosol flow ratio of 10. For the campaign, the average sampling temperature and pressure as measured by the CCNC sensors were (23.7±1.4) °C and (1006±6) hPa (posititve deviation from ambient pressure due to measurement uncertainties; Rose et al., 2010b). The effective water vapor supersaturation (S) was regulated by the temperature difference between the upper and lower end of the CCNC flow column (ΔT) and calibrated as described below and in Rose et al. (2008).

For each CCN measurement cycle, ΔT was set to 5 different levels in the range of 1.98–16.9 K corresponding to S values of 0.068% to 1.27%. For each ΔT and S, respectively, the diameter of the dry aerosol particles selected by the DMA (D) was set to 9 different values in the range of 20–290 nm. At each D, the number concentration of total aerosol particles (condensation nuclei, CN), N_{CN}, was measured with the CPC, and the number concentration of CCN, N_{CCN}, was measured with the CCNC. The integration time for each measurement data point was 30 s, the recording of a CCN efficiency spectrum (N_{CCN}/N_{CN} vs. D) took ∼16 min (including 50 s adjustment time for each new particle size and 4 min for adjustment to the next supersaturation level), and the completion of a full measurement cycle comprising CCN efficiency spectra at 5 different supersaturation levels

Table 1. Characteristic parameters from the 5 calibration experiments performed during the campaign (arithmetic mean ± standard deviation). The last column shows the maximum relative deviation of individual calibration data points from the average calibration line (S vs. ΔT), indicating maximum relative uncertainties in S.

ΔT [K]	D_a [nm]	S [%]	$\Delta S/S$ [%]
1.99±0.02	158.8±5.2	0.072±0.004	6.9
4.46±0.01	66.7±1.9	0.28±0.01	5.8
10.70±0.02	35.3±1.0	0.75±0.04	5.9
14.44±0.01	28.2±0.8	1.06±0.05	6.7
16.95±0.02	24.9±0.7	1.29±0.06	6.7

took ∼85 min (including 5 min for adjustment between the highest and lowest level of S).

2.2.2 Calibration of CCN counter

With respect to the effective water vapor supersaturation S, the CCNC was calibrated with ammonium sulfate aerosol as described by Rose et al. (2008). During the campaign, five calibration experiments were performed, and in each of these experiments multiple CCN efficiency spectra were recorded for 5 different ΔT values. The midpoint activation diameter of each CCN efficiency spectrum was taken as the critical dry diameter for the CCN activation of ammonium sulfate particles, and the corresponding critical supersaturation was calculated with an activity parameterization Köhler model (AP3; Rose et al., 2008) that can be regarded as the most accurate reference available. Note that other frequently used Köhler models and the corresponding calibration lines would deviate by up to 20% or more, and care has to be taken when comparing the results of different CCN measurement and model studies (Rose et al., 2008). The calculated critical supersaturation was taken as the effective supersaturation at the given ΔT value.

Figure 1 shows the average CCN efficiency spectra obtained from the 5 calibration experiments with ammonium sulfate aerosol, and the corresponding average calibration parameters are given in Table 1. A linear least-squares fit to the data pairs of S and ΔT was taken as the CCNC calibration line for the entire campaign: $S=k_s\Delta T+S_0$ with k_s=0.08041% K^{-1} and S_0=−0.09109%, R^2=0.9929. It was applied to calculate S from the average value of ΔT recorded during each measurement of a CCN efficiency spectrum of atmospheric aerosol. As detailed by Rose et al. (2008), variations in S are mostly due to variations of the CCNC inlet temperature. The standard deviations of the calibration data points and their maximum deviations from the calibration line ($\Delta S/S$) as listed in Table 1 indicate a relative uncertainty of less than ∼7% for S in the CCN measurements reported in this study.
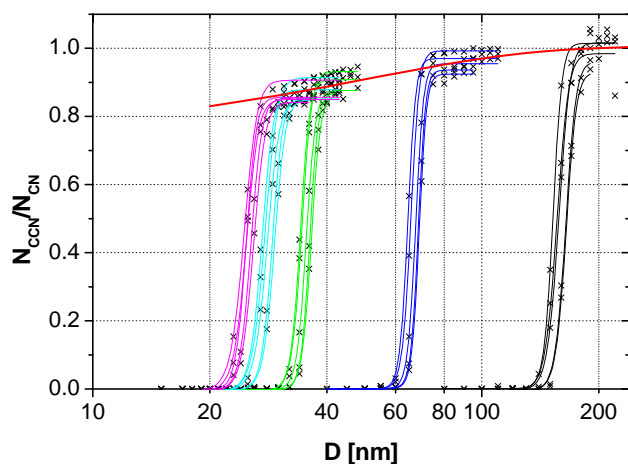
Fig. 1. CCN efficiency spectra obtained from 5 calibration experiments with ammonium sulfate aerosol performed during the campaign (data points and CDF fits). Different colors indicate the different supersaturation levels. The red line is the asymptotic function that was used to correct for different counting efficiencies of the CPC and the CCNC (f_{corr}).

2.2.3 Correction of measured CCN efficiency spectra

The measured atmospheric CCN efficiency spectra were corrected for multiply charged particles as described by Frank et al. (2006) and for the DMA transfer function as described by Rose et al. (2008). For the multiple charge correction we used the total aerosol particle number size distributions measured in parallel with the TDMPS. For several days TDMPS data were not available, and no charge correction was performed. Nevertheless, the CCN data from these days remained comparable with the others, because the effects of the charge correction were generally small (<5% change in activation diameters and other parameters used for further analysis).

The CCN efficiency spectra were also corrected for the differences in the counting efficiencies of the CCNC and the CPC. If the CCNC and CPC counting efficiencies were the same, a maximum activated fraction of $N_{CCN}/N_{CN} \approx 1$ would be expected for ammonium sulfate calibration aerosol particles at all supersaturation levels. As illustrated in Fig. 1, however, the measured maximum value of N_{CCN}/N_{CN} was close to one only for larger particles. For smaller particles the measured maximum levels of N_{CCN}/N_{CN} decreased with decreasing particle size, which can be attributed to a decrease in the counting efficiency of the CCNC (most likely due to wall losses in the tubing inside the instrument). To correct for this bias, we have fitted an asymptotic function to those data points of the calibration efficiency spectra that reached at least 95% of their respective maximum values (red line in Fig. 1): $f_{corr} = x_1 - x_2 \cdot x_3^D$ with $x_1 = 1.00547$, $x_2 = 0.26208$, $x_3 = 0.98024$, $R^2 = 0.70881$. The inverse of this correction function was multiplied with all the atmospheric N_{CCN}/N_{CN}

data points after the charge and before the transfer function corrections. In the preceding discussion paper, the counting efficiency correction was performed after the charge and transfer function correction. On average the change in the sequence of corrections had little effect on the results (deviations <1% for D_a and MAF, ~4% for σ), but the data analysis with the counting efficiency before the transfer function correction was more robust (fewer cases where CDF fits did not converge). In the following, for simplicity, the corrected CCN efficiency spectra are referred to as the "measured" CCN efficiency spectra. Note that all CCN efficiency spectra presented in the figures of this paper show the corrected ones.

The scattering of the highest N_{CCN}/N_{CN} measurement values around the counting efficiency correction function determined in the calibration experiments (f_{corr}, Fig. 1) indicate a relative uncertainty of ~5% for the CCN efficiencies determined for atmospheric aerosols (corrected CCN efficiency spectra). For the period after 20 July the relative uncertainty increased to ~10%, as indicated by a decrease in the observed maximum CCN efficiencies (offset in the CCNC flow rate).

2.2.4 Parameters derived from the CCN efficiency spectra

Basic spectral parameters

The measured CCN efficiency spectra were fitted with a cumulative Gaussian distribution function (CDF; Rose et al., 2008):

$$f_{N_{CCN}/N_{CN}} = a\left(1 + \mathrm{erf}\left(\frac{D - D_a}{\sigma_a \sqrt{2}}\right)\right) \quad (1)$$

The following best-fit parameters were determined for each spectrum: the maximum activated fraction $MAF_f = 2a$, the midpoint activation diameter D_a, and the CDF standard deviation σ_a. In addition to the 3-parameter CDF fits with varying a, D_a, and σ_a, we have also performed 2-parameter CDF fits which were forced to $MAF_f = 1$ by fixing the parameter a at 0.5 and varying only D_a and σ_a. For the midpoint activation diameters and CDF standard deviations obtained from these fits we use the symbols D_t and σ_t. In addition to the above CDF fit-based parameters, the CCN efficiency measured at the largest diameter of each spectrum (D_{max}) was also taken for further analysis and discussion: $MAF_m = N_{CCN}/N_{CN}$ at $D_{max} \approx 270$ nm.

Characteristic examples of atmospheric CCN efficiency spectra of atmospheric aerosols and the corresponding CDF fits and parameters are illustrated in Fig. 2. Figure 2a shows an "ideal" spectrum that is characteristic for internally mixed aerosols with homogeneous composition and hygroscopicity of the particles (similar to ammonium sulfate calibration aerosol). In this case, the observed CCN efficiencies reach up to one ($MAF_f \approx MAF_m \approx 1$), and the activation diameters

and standard deviations derived from the 3-parameter and 2-parameter CDF fits are essentially the same ($D_a \approx D_t$; $\sigma_a \approx \sigma_t$).

At medium and high supersaturation (S=0.47–1.27%), most CCN efficiency spectra were qualitatively similar to the one in Fig. 2a. At low supersaturation (S=0.068–0.27%), however, most CCN efficiency spectra deviated from the ideal shape of a completely internally mixed aerosol and looked like the exemplary spectrum displayed in Fig. 2b, which is characteristic for externally mixed aerosols.

In these cases, the highest observed CCN efficiencies remain well below one (MAF<1), which indicates an external mixture of CCN-active particles with CCN-inactive particles, whereby the difference in CCN activity is due to chemical composition and hygroscopicity (not particle size). Test experiments with different CCNC flow rates yielded the same result, indicating that the observed deviations of MAF from unity were not governed by potential kinetic limitations of water uptake in the CCNC.

For CCN efficiency spectra with MAF<1 the activation diameters and standard deviations derived from the 3-parameter and 2-parameter CDF fits are not the same: the 3-parameter fit results represent the average properties of the CCN active aerosol particle fraction, whereas the 2-parameter fit results approximate the overall properties of the external mixture of CCN-active and CCN-inactive particles.

The difference between unity and the maximum observed CCN efficiency (1–MAF_m or 1–MAF_f, respectively) represents the fraction of externally mixed CCN-inactive particles at D_{max} or averaged over the diameter range of D_a to D_{max}, respectively. The CDF standard deviations are general indicators for the extent of external mixing and heterogeneity of particle composition in the investigated aerosol: σ_a characterizes the CCN-active particles in the size range around D_a, and σ_t characterizes the overall heterogeneity of CCN-active and -inactive particles in the size range around D_t. Under ideal conditions, the CDF standard deviations should be zero for an internally mixed, fully monodisperse aerosol with particles of homogeneous chemical composition. Even after correcting for the DMA transfer function, however, calibration aerosols composed of high-purity ammonium sulfate exhibit small non-zero σ_a values that correspond to ~3% of D_a and can be attributed to heterogeneities of the water vapor supersaturation profile in the CCNC or other non-idealities such as DMA transfer function and particle shape effects (Rose et al., 2008). Thus, normalized CDF standard deviations or "heterogeneity parameter" values of $\sigma_a/D_a \approx 3\%$ indicate internally mixed CCN, whereas higher values indicate external mixtures of particles with varying chemical composition and hygroscopicity.

In addition to the activation diameters derived from the CCN efficiency spectra, we have also determined an apparent cut-off diameter of CCN activation D_{cut}. It is the diameter above which the integral CN number concentration equals the observed CCN concentration ($N_{CCN,S}$ as detailed below). Note that unlike D_a and D_t, the determination of
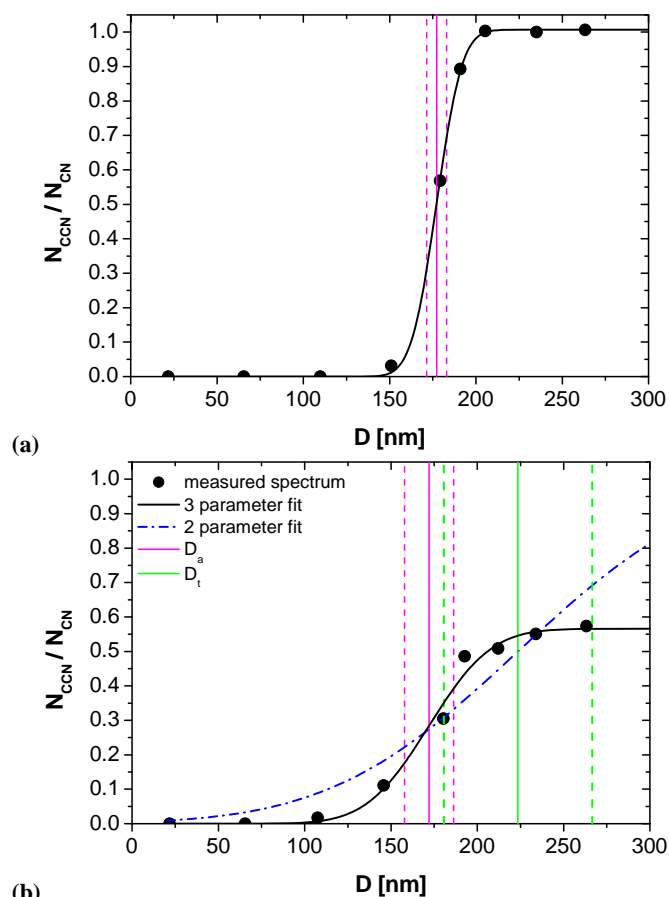
Fig. 2. Exemplary CCN efficiency spectra **(a)** with "ideal" shape (12 July 2006, 18:55–19:06), and **(b)** with low maximum fraction of activated particles (9 July 2006, 03:23–03:34): measurement data points (corrected according to Sect. 2.2.3; black dots); 3-parameter CDF fit (black solid line) with fit parameters D_a (pink line), and σ_a (distance between pink dashed lines); 2-parameter CDF fit (blue dash-dotted line) with fit parameters D_t (green line) and σ_t (distance between green dashed lines).

D_{cut} requires knowledge of the CN size distribution and the assumption of a sharp cut-off (corresponding to σ_t=0). A list of frequently used symbols is given in Table A1 at the end of the manuscript.

Effective hygroscopicity parameters

As proposed by Petters and Kreidenweis (2007), an effective hygroscopicity parameter κ can be used to describe the influence of chemical composition on the CCN activity of aerosol particles, i.e. on their ability to absorb water vapor and act as CCN. Based on Köhler theory, κ relates the dry diameter of aerosol particles to the critical water vapor supersaturation, i.e. the minimum supersaturation required for cloud droplet formation. For a given supersaturation,

κ allows calculating the critical dry particle diameter, i.e. the minimum diameter required for the particle to be CCN-active. According to measurements and thermodynamic models, κ is zero for insoluble materials like soot or mineral dust, $\sim$0.1 for secondary organic aerosols, $\sim$0.6 for ammonium sulfate and nitrate, $\sim$0.95–1 for sea salt (obtained from ρ_{ion} values in Niedermeier et al., 2008), and 1.28 for sodium chloride aerosols. The effective hygroscopicity of mixed aerosols can be approximated by a linear combination of the κ-values of the individual chemical components weighted by the volume or mass fractions, respectively (Kreidenweis et al., 2008; Gunthe et al., 2009). On average, continental and marine aerosols tend to cluster around κ=0.3 and κ=0.7, respectively (Andreae and Rosenfeld, 2008; Kreidenweis et al., 2009; Pöschl et al., 2009). Laboratory experiments with biomass burning aerosols yielded κ values ranging from 0.02 to 0.8 (Petters et al., 2009).

For all data pairs of supersaturation and activation diameter derived from the CCN efficiency spectra measured in this study, κ parameters were calculated from the following Köhler model equation (equivalent to Eq. 6 of Petters and Kreidenweis, 2007, and Eq. A30 of Rose et al., 2008):

$$s = \frac{D_{wet}^3 - D^3}{D_{wet}^3 - D^3(1-\kappa)} \exp\left(\frac{4\,\sigma_{sol}\,M_w}{R\,T\,\rho_w\,D_{wet}}\right) \quad (2)$$

κ was determined by inserting the observed activation diameter (D_a, D_t, or D_{cut}) for D and varying both κ and the droplet diameter D_{wet} until the saturation ratio s was equivalent at the same time to the prescribed supersaturation S and to the maximum of a Köhler model curve of CCN activation (numerical minimum search for $-s$ and for $|s-(1+S/100\%)|$ with Matlab "fminsearch" and start values of κ=0.2 and D_{wet}=D).

For the temperature we inserted T=298.15 K, the droplet surface tension was approximated by that of water (σ_{sol}=0.072 J m^{-2}), and the other parameters were set to R=8.315 J K^{-1} mol^{-1} (gas constant), ρ_w=997.1 kg m^{-3} and M_w=0.018015 kg mol^{-1} (density and molar mass of water). Note that κ values derived from CCN measurement data through Köhler model calculations assuming the surface tension of pure water have to be regarded as "effective hygroscopicity parameters" that account not only for the reduction of water activity by the solute ("effective Raoult parameters") but also for surface tension effects. For more information see Petters and Kreidenweis (2007); Gunthe et al. (2009); Mikhailov et al. (2009); Pöschl et al. (2009). The parameter κ_a calculated from the data pairs of S and D_a characterizes the average hygroscopicity of CCN-active particles in the size range around D_a. κ_t calculated from D_t is an approximate measure (proxy) for the effective hygroscopicity of CCN-active and -inactive particles in the size range around D_t. Accordingly, κ_t is better suited for comparison with average κ values calculated from

H-TDMA data and for the calculation of CCN number concentrations when CCN-active particles are externally mixed with CCN-inactive particles. On the other hand, κ_a is better suited for comparison with κ values predicted from AMS measurements, because κ_a is not influenced by CCN-inactive particles consisting mostly of insoluble and refractory materials like mineral dust and soot (or biopolymers that tend to char upon heating), which are not (or less efficiently) detected by AMS. The parameter κ_{cut} calculated from the data pairs of S and D_{cut} characterizes the effective average hygroscopicity of CCN-active particles in the size range above D_{cut}. D_{cut} and κ_{cut} can also be determined from the results of integrated CCN concentration measurements of polydisperse aerosols, and may thus be useful for comparison with studies lacking size-resolved CCN data.

CCN size distributions and number concentrations

CCN size distributions ($dN_{CCN}/d\log D$) were calculated by multiplying the CCN efficiency spectra (3-parameter CDF fits of N_{CCN}/N_{CN}) with the total aerosol particle (CN) number size distributions measured in parallel ($dN_{CN}/d\log D$). In these calculations, the fit parameter a was limited to a maximum value of 0.5 (MAF$_f$=1), because CCN concentrations exceeding CN concentrations are physically not realistic. Additional test calculations with a not limited to 0.5 led to total CCN concentrations that were on average less than 1% higher.

Near the activation diameter, the size resolution of the CCN efficiency spectra was generally higher than that of the CN size distribution measurement data from the TDMPS ($d\log D$=0.083). Thus the CN size distributions were linearly interpolated on a grid with ten-fold smaller size steps.

Total CCN concentrations ($N_{CCN,S}$) were calculated by stepwise integration of the CCN size distributions with $d\log D$=0.0083 from 3 to 900 nm. Note that insufficient size-resolution near the activation diameter can lead to substantial deviations in the calculation of total CCN number concentrations (up to $\sim$10% at low S, up to $\sim$5% at high S with $d\log D$=0.083 vs. $d\log D$=0.0083 in this study).

3 Results and discussion

3.1 CCN efficiency spectra and related parameters

During the 30 day campaign period of PRIDE-PRD2006, we measured $\sim$2200 size-resolved CCN efficiency spectra (activation curves) for atmospheric aerosols at water vapor supersaturations in the range of 0.068% to 1.27%. Exemplary spectra are shown in Fig. 2, and the derivation and interpretation of characteristic parameters is explained in Sect. 2.2.4.
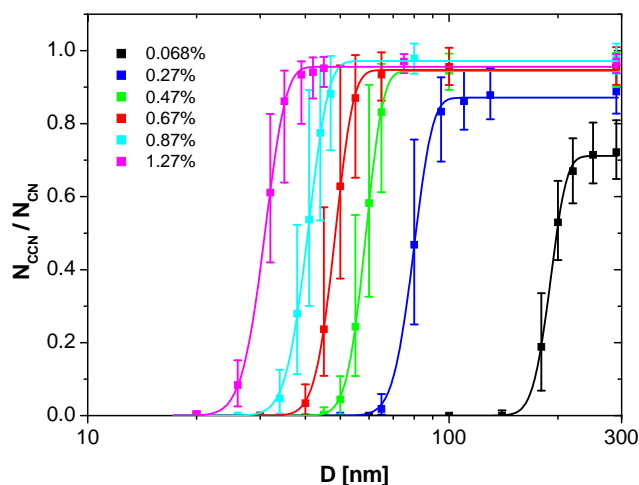
Fig. 3. CCN efficiency spectra at S=0.068%–1.27% averaged over the entire campaign. The data points are median values calculated from the CDF fits to all measured spectra at the particle diameters initially selected with the DMA (20–290 nm). The error bars extend from the lower to the upper quartile, and the lines are 3-parameter CDF fits to the data points (Sect. 2.2.4).

3.1.1 Campaign averages

Figure 3 shows campaign averages of the atmospheric CCN efficiency spectra at the six investigated supersaturation levels. The average parameters derived from the CCN efficiency spectra are summarized in Table 2.

As expected, the midpoint activation diameters D_a increased with S and were larger than the critical dry diameters for CCN activation of pure ammonium sulfate particles at the same supersaturation levels. At medium and high supersaturation (S=0.47–1.27%), the CCN efficiency spectra generally reached up to one (MAF$_f$≈1) and the relative standard deviations of the 3-parameter CDF fits were small (σ_a/D_a≈10%), which implies that nearly all aerosol particles larger than the midpoint activation diameter ($D > D_a$) were CCN-active. At low supersaturation (S=0.068–0.27%), however, the maximum activated fractions remained on average well below one, which indicates a substantial portion (1−MAF$_f$) of externally mixed CCN-inactive particles with much lower hygroscopicity. At S=0.068%, the average MAF$_f$ was only ∼0.75 with minimum values as low as ∼0.4, i.e. even at diameters as large as ∼250 nm an average of ∼25% and up to ∼60% of the aerosol particles were not CCN-active. To our knowledge such high portions of externally mixed CCN-inactive particles have not been observed before in atmospheric aerosols.

Sensitivity tests with the κ-Köhler model described in Sect. 2.2.4 (Petters and Kreidenweis, 2007) indicate that particles as large as ∼300 nm must have an effective hygroscopicity parameter $\kappa < 0.1$ to not be activated at S=0.068%. On the other hand, S≈0.7% would be required to activate
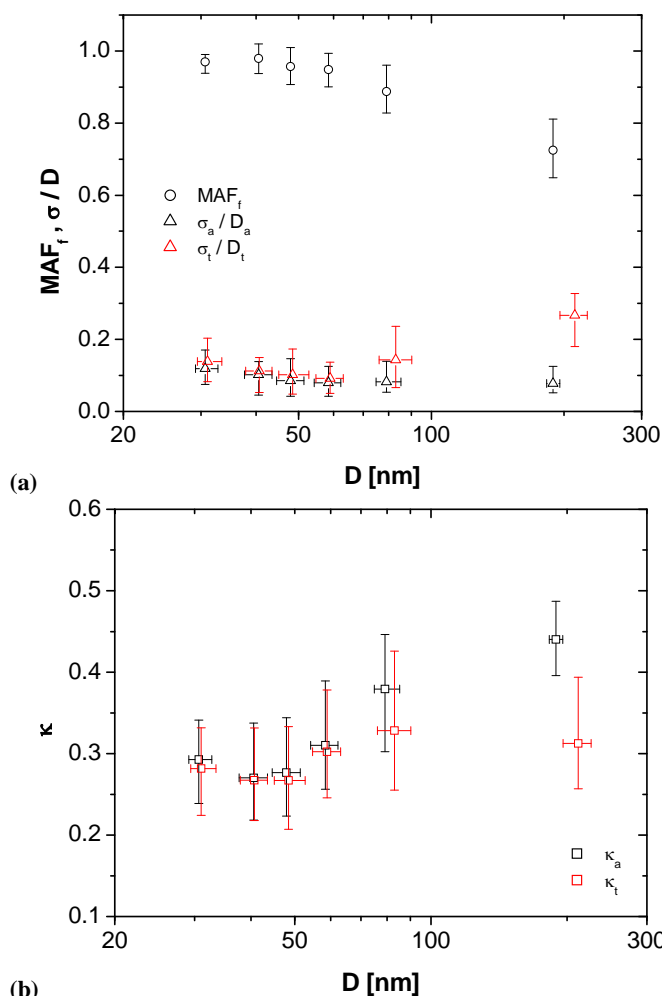
Fig. 4. Characteristic parameters derived from the CCN efficiency spectra averaged over the entire campaign: **(a)** maximum activated fractions (MAF$_f$) and heterogeneity parameters (σ_a/D_a, σ_t/D_t); **(b)** hygroscopicity parameters (κ_a, κ_t) plotted against the midpoint activation diameter (D_a or D_t, respectively). The data points are median values corresponding to a given level of supersaturation, and the error bars extend to lower and upper quartiles.

300 nm particles that are wettable but completely insoluble and non-hygroscopic (κ=0). Most likely the CCN-inactive particles were freshly emitted (non-aged/non-coated) soot particles with κ≈0.01, which will be discussed further in a follow-up study based on Volatility Tandem DMA (VT-DMA) and chemical composition data (Rose et al., 2010a). Other recent studies from PRIDE-PRD2006 (Garland et al., 2008) and a similar field campaign in the vicinity of Beijing (Cheng et al., 2009; Garland et al., 2009; Wehner et al., 2009; Wiedensohler et al., 2009) also indicate strong regional pollution with large proportions of externally mixed soot particles in the atmospheric aerosol near Chinese mega-cities and city-clusters.

Table 2. Characteristic average CCN parameters (arithmetic mean values ± standard deviation) for the entire campaign, for the Biomass Burning Event (BBE, 23–26 July) and for the campaign excluding the BBE for different S. Quantities are midpoint activation diameters (D_a, D_t, D_{cut}), maximum activated fractions (MAF$_f$, MAF$_m$), CDF standard deviations (σ_a, σ_t), heterogeneity parameters (σ_a/D_a, σ_t/D_t), hygroscopicity parameters (κ_a, κ_t, κ_{cut}), number concentrations of total aerosol particles (3–900 nm, $N_{CN,tot}$) and of cloud condensation nuclei ($N_{CCN,S}$), and ratio of $N_{CN,tot}$ to $N_{CCN,S}$ as defined in Sect. 2.2.4. n_{ES} and n_{SD} are the numbers of averaged CCN efficiency spectra and size distributions, respectively.

S [%]	D_a [nm]	D_t [nm]	D_{cut} [nm]	MAF$_f$	MAF$_m$	σ_a [nm]	σ_t [nm]	σ_a/D_a	σ_t/D_t
Entire campaign									
0.068	189.5±11.3	213.1±21.8	216.8±19.2	0.73±0.12	0.73±0.13	17.3±10.0	55.3±26.3	0.09±0.05	0.25±0.10
0.27	81.4±9.0	85.0±11.2	89.8±13.3	0.89±0.09	0.93±0.10	8.8±6.9	13.8±10.1	0.10±0.07	0.15±0.10
0.47	59.4±7.0	60.5±8.1	64.4±9.3	0.95±0.07	0.98±0.08	5.7±4.8	6.7±5.8	0.09±0.06	0.10±0.07
0.67	48.9±6.0	49.7±6.8	52.8±8.5	0.95±0.07	0.99±0.08	5.2±4.4	6.3±5.3	0.10±0.07	0.12±0.08
0.87	40.9±4.4	41.3±5.1	44.5±7.3	0.98±0.06	1.00±0.08	4.2±2.9	4.7±3.4	0.10±0.06	0.11±0.07
1.27	31.5±3.5	31.9±3.5	39.2±10.3	0.96±0.05	1.02±0.06	4.2±2.7	4.8±2.9	0.13±0.07	0.15±0.08
BBE									
0.068	204.8±12.2	222.3±21.4	234.8±21.3	0.75±0.09	0.76±0.10	17.8±9.9	43.4±19.2	0.09±0.05	0.19±0.08
0.27	93.3±11.9	98.9±13.2	107.3±15.6	0.87±0.10	0.92±0.10	17.6±9.1	23.7±9.4	0.18±0.09	0.23±0.08
0.47	68.7±9.2	71.4±10.3	77.9±9.4	0.92±0.05	0.96±0.05	11.8±6.3	14.2±7.3	0.16±0.07	0.19±0.08
0.67	59.3±7.1	62.8±8.0	69.4±8.0	0.91±0.06	0.94±0.06	12.0±4.6	15.8±7.0	0.20±0.06	0.24±0.08
0.87	46.5±5.4	48.2±7.1	55.5±8.2	0.94±0.05	0.98±0.06	7.3±3.8	8.8±4.8	0.15±0.08	0.18±0.09
1.27	33.9±4.9	35.0±4.6	51.3±13.4	0.92±0.07	0.99±0.03	5.6±3.7	7.3±3.4	0.16±0.09	0.20±0.09
Entire campaign excluding BBE									
0.068	187.4±9.4	211.8±21.5	213.6±17.1	0.73±0.13	0.73±0.14	17.3±10.1	56.9±26.7	0.09±0.05	0.26±0.11
0.27	79.8±7.2	83.1±9.5	86.8±10.2	0.89±0.09	0.93±0.10	7.7±5.6	12.5±9.5	0.09±0.06	0.14±0.10
0.47	58.3±5.8	59.1±6.6	62.2±7.3	0.95±0.07	0.98±0.08	4.9±4.0	5.7±4.9	0.08±0.06	0.09±0.06
0.67	48.0±5.0	48.6±5.3	51.1±6.4	0.96±0.07	0.99±0.08	4.6±3.8	5.4±4.2	0.09±0.07	0.11±0.08
0.87	40.2±3.7	40.4±4.0	42.7±5.3	0.98±0.06	1.01±0.08	3.9±2.5	4.2±2.8	0.09±0.06	0.10±0.06
1.27	31.0±2.9	31.2±2.9	35.6±5.5	0.97±0.04	1.03±0.06	3.9±2.3	4.3±2.5	0.12±0.06	0.13±0.07

S [%]	κ_a	κ_t	κ_{cut}	$N_{CN,tot}$ [cm^{-3}]	$N_{CCN,S}$ [cm^{-3}]	$N_{CCN,S}/N_{CN,tot}$	n_{ES}	n_{SD}
Entire campaign								
0.068	0.44±0.08	0.33±0.10	0.30±0.08		995±745	0.06±0.05	429	331
0.27	0.37±0.10	0.33±0.11	0.29±0.11		6531±3974	0.36±0.16	428	331
0.47	0.32±0.09	0.30±0.09	0.26±0.10		9649±5214	0.53±0.19	433	337
0.67	0.28±0.09	0.27±0.09	0.24±0.10		10731±5991	0.59±0.20	299	230
0.87	0.28±0.08	0.28±0.09	0.23±0.09		12967±6385	0.71±0.18	421	327
1.27	0.29±0.09	0.28±0.08	0.18±0.09		15839±5602	0.85±0.10	123	97
all	0.34±0.11	0.30±0.10	0.26±0.10	18150±7991			2133	1653
BBE								
0.068	0.35±0.06	0.28±0.07	0.24±0.06		1899±1157	0.14±0.06	51	49
0.27	0.25±0.09	0.21±0.09	0.17±0.07		7041±3753	0.46±0.16	50	49
0.47	0.21±0.08	0.19±0.08	0.14±0.05		8977±4448	0.59±0.16	48	46
0.67	0.16±0.06	0.13±0.06	0.10±0.04		8170±5648	0.54±0.12	24	22
0.87	0.19±0.07	0.18±0.07	0.12±0.06		11565±5793	0.73±0.15	47	45
1.27	0.25±0.13	0.22±0.11	0.08±0.06		13486±4171	0.85±0.07	22	22
all	0.24±0.10	0.21±0.09	0.15±0.08	15178±6479			242	233
Entire campaign excluding BBE								
0.068	0.46±0.07	0.33±0.10	0.32±0.08		838±506	0.05±0.03	378	282
0.27	0.39±0.09	0.35±0.11	0.31±0.10		6442±4011	0.34±0.16	378	282
0.47	0.33±0.08	0.32±0.09	0.28±0.09		9755±5324	0.52±0.19	385	291
0.67	0.29±0.08	0.28±0.08	0.25±0.09		11002±5975	0.60±0.21	275	208
0.87	0.29±0.08	0.29±0.08	0.25±0.09		13191±6456	0.70±0.19	374	282
1.27	0.30±0.07	0.29±0.07	0.21±0.08		16529±5801	0.85±0.10	101	75
all	0.35±0.10	0.31±0.09	0.28±0.10	18638±8111			1891	1420

Figure 4a gives an overview of the maximum activated fractions (MAF$_f$) and normalized standard deviations (σ_a/D_a) of the 3-parameter CDF fits as well as the normalized standard deviations of the 2-parameter CDF fits (σ_t/D_t) to the measured CCN efficiency spectra. The average parameter values are plotted against the corresponding average midpoint activation diameters (D_a, D_t) that have been observed at the six prescribed levels of water vapor supersaturation (S=0.068–1.27%).

As detailed in Sect. 2.2.4, σ_a/D_a characterizes the heterogeneity of CCN-active particles in the size range around D_a, whereas σ_t/D_t characterizes the overall heterogeneity of aerosol particles in the size range around D_t.

For small particles in the nucleation or Aitken size range ($\sim$30–70 nm), the heterogeneity parameters σ_a/D_a and σ_t/D_t were nearly identical and close to $\sim$10%. This is clearly higher than the $\sim$3% observed for aerosols of homogeneous chemical composition (e.g. pure ammonium sulfate), indicating that the particles in this size range were not fully internally mixed with respect to their solute content. For larger particles in the accumulation size range ($\sim$70–200 nm), σ_a/D_a remained at $\sim$10% whereas σ_t/D_t increased strongly up to $\sim$25% at $\sim$200 nm. This confirms that the CCN-active particles in the accumulation size range had fairly homogeneous properties but were externally mixed with CCN-inactive particles.

Figure 4b gives an overview of the effective hygroscopicity parameters (κ_a, κ_t) that have been derived from the midpoint activation diameters (D_a, D_t) of the 3-parameter and 2-parameter CDF fits, respectively. As detailed in Sect. 2.2.4, κ_a calculated from S and D_a characterizes the average hygroscopicity of CCN-active particles in the size range around D_a, whereas κ_t calculated from S and D_t is a proxy for the effective hygroscopicity of mixtures of CCN-active and -inactive particles in the size range around D_t.

For small particles in the nucleation or Aitken size range ($\sim$30–70 nm), κ_a and κ_t were nearly identical and close to $\sim$0.3. For larger particles in the accumulation size range ($\sim$70–200 nm), however, κ_a increased substantially to $\sim$0.4–0.5, whereas κ_t increased only slightly to $\sim$0.33.

Overall, larger particles were on average more hygroscopic but also more heterogeneous than smaller particles. The observed values of κ_a, κ_t, σ_a/D_a, σ_t/D_t, and MAF$_f$ suggest that the particles in the nucleation or Aitken size range were composed mostly of organics and sulfate and were largely but not fully internally mixed, whereas the particles in the accumulation size range consisted mostly of an external mixture of soot particles ($\kappa < 0.1$; $\sim$25% at $\sim$200 nm) and sulfate-rich particles ($\kappa \approx 0.4$–0.5; $\sim$75% at $\sim$200 nm). Note that the properties of large accumulation mode particles are not only important for cloud formation at low and medium supersaturation (low and moderate updraft velocities; Segal and Khain, 2006; Reutter et al., 2009) but also for aerosol optical properties and direct radiative effects on climate (Garland et al., 2008). These and other aspects

of aerosol chemical composition and mixing state will be explored further and discussed in more detail in a follow-up study (Rose et al., 2010a). Averaged over all diameters, the mean hygroscopicity parameter values for the entire campaign were κ_a=0.34 and κ_t=0.30 (Table 2). The hygroscopicity parameter related to the cut-off diameter D_{cut} (κ_{cut}) was on average 10% smaller than κ_t and had an arithmetic mean value of 0.26.

3.1.2 Time series and biomass burning event

Figure 5 shows the time series of characteristic parameters (D_a, D_t, κ_a, κ_t, σ_a, σ_t, σ_a/D_a, σ_t/D_t, MAF$_f$, MAF$_m$) derived from the atmospheric CCN efficiency spectra measured throughout the campaign. For clarity, the parameters in Fig. 5c–j are shown only for the smallest and largest supersaturations that were measured during the entire campaign (S=0.068%, S=0.87%). The temporal evolution of most parameters at S=0.068% was qualitatively similar to S=0.27%, and that at S=0.87% was representative for S=0.47–1.27%.

Most parameters exhibited pronounced diurnal cycles which are consistent with the results of other recent studies from PRIDE-PRD2006 (Garland et al., 2008; Hua et al., 2008b). The diurnal cycles in CCN properties will be described and discussed together with the variability of other aerosol properties including chemical composition, volatility, and optical parameters in a follow up study (Rose et al., 2010a). As illustrated in Fig. 5i and j, both the fitted and the measured maximum activated fractions (MAF$_f$, MAF$_m$) dropped by $\sim$10% after 20 July, which is most likely due to a measurement artifact (offset in the flow rate of the CCNC).

In addition to the diurnal variability, several CCN parameters exhibited pronounced changes during high pollution events. Especially on 23–26 July, the midpoint activation diameters and standard deviations of the CDF fits increased and the hygroscopicity parameters decreased relative to the campaign average (Fig. 5, panels a–h). The changes indicate an increase in the portion of particulate matter with low hygroscopicity (organic substances) and in the heterogeneity of particles (external mixing), and they were most pronounced for small particles ($\sim$30–80 nm; $S \geq 0.27\%$).

The highly polluted period of 23–26 July 2006 was characterized by intense local biomass burning and very high aerosol mass concentrations (Garland et al., 2008). During this period, the source of the pollution was evident and unique: the burning of plant waste by local farmers was visible in the vicinity surrounding the measurement site, and it was the only time that such intense local biomass burning and pollution occurred during the campaign. The heavy biomass burning event started after a power outage in the evening of 22 July and ended by heavy rainfalls beginning at $\sim$13:00 on 26 July. Thus the period of 23 July, 00:00–26 July, 12:59 will be referred to as the "Biomass Burning Event (BBE)". The average CCN parameters for this period are summarized in Table 2.
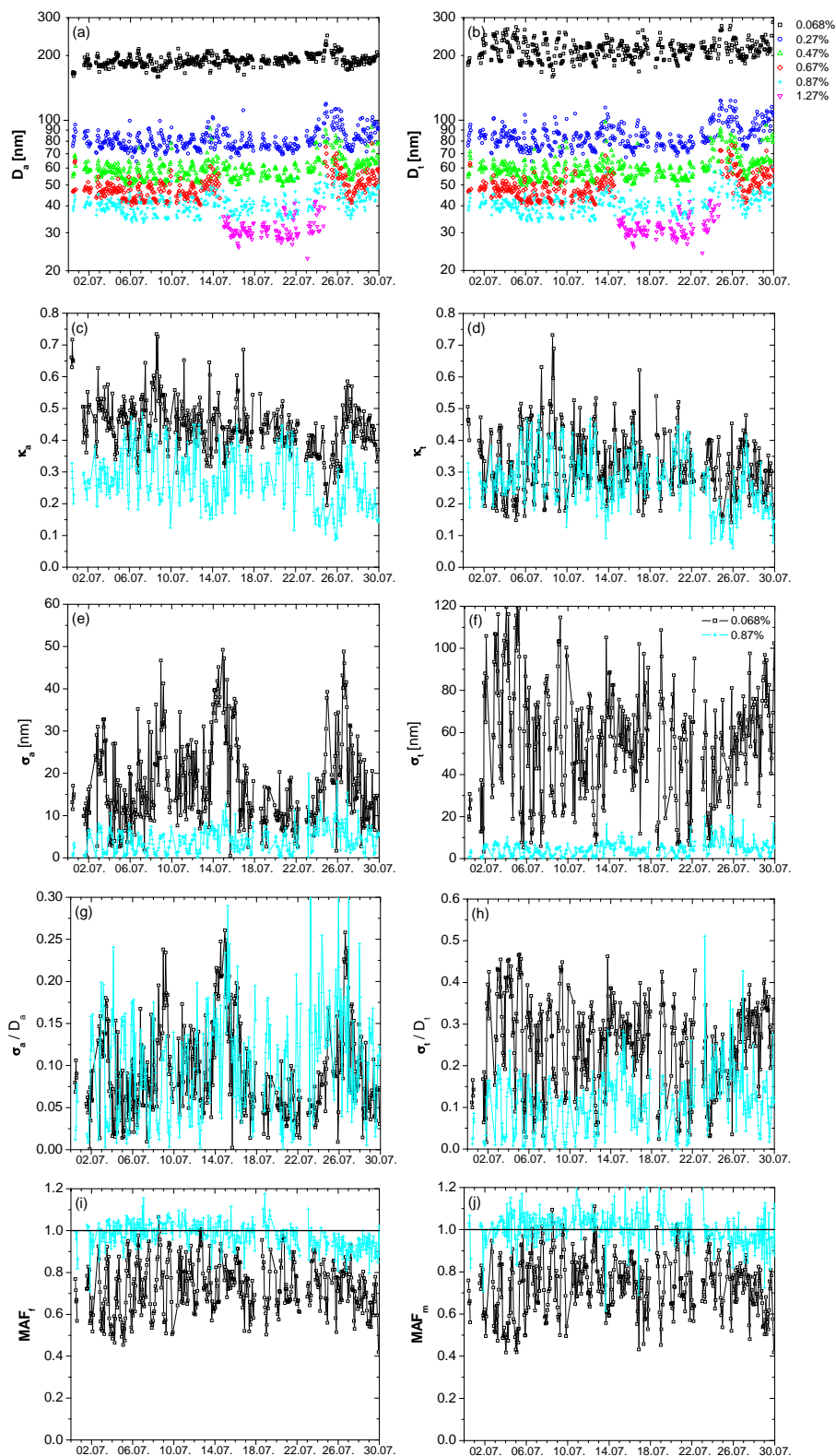
Fig. 5. Time series of the characteristic parameters derived from the CCN efficiency spectra measured at different supersaturations plotted against the date in July 2006.

During the BBE, the CCN efficiency spectra were shifted towards larger particle sizes for all supersaturations, reflecting lower CCN activity than during the rest of the campaign. The increase of D_a was most pronounced for S=0.67% (+22% during the BBE) and least different for S=0.068% and S=1.27% (+8% during the BBE). Moreover, for all supersaturations, except 0.068%, the standard deviations of the CDF fits and heterogeneity parameters (σ/D), increased by factors up to $\sim$2, indicating a strong increase in the heterogeneity of small particles (30–100 nm, Table 2). Only the maximum activated fractions did not change significantly during the biomass burning event, i.e. the externally mixed fraction of particles that could not be activated at low S remained the same.

Figure 6 gives an overview of the effective hygroscopicity parameters (κ_a, κ_t) that have been derived from the midpoint activation diameters (D_a, D_t) averaged over the entire campaign and over the biomass burning event. Figure 6a shows that during the BBE the average hygroscopicity of CCN-active particles was substantially reduced at all sizes. Averaged over all diameters, the mean value of κ_a during the BBE was $\sim$30% lower than during the rest of the campaign: 0.24 vs. 0.34 (Table 2).

As illustrated in Fig. 6b, the average hygroscopicity of the total aerosol, including CCN-active and -inactive particles, was also strongly reduced for small particles ($<$100 nm) but not so much for large particles ($\sim$200 nm). Averaged over all diameters, however, the mean value of κ_t during the BBE was also $\sim$30% lower than during the rest of the campaign: 0.21 vs. 0.30 (Table 2).

To our knowledge, these are the first size-resolved CCN field measurement data and hygroscopicity parameters reported for freshly emitted biomass burning smoke in the atmosphere. They are consistent with earlier lab studies reporting low hygroscopicity of freshly emitted biomass burning particles (Rissler et al., 2006; Andreae and Rosenfeld, 2008; Petters et al., 2009).

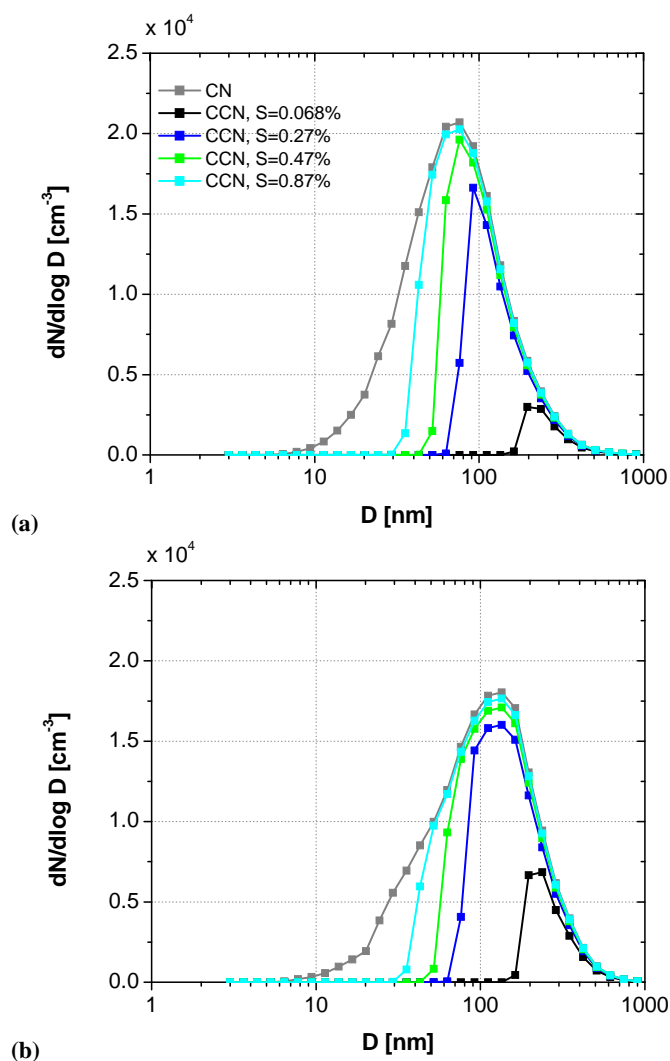## 3.2 CCN size distributions and number concentrations

Figure 7 shows total aerosol particle (CN) and CCN number size distributions averaged over the entire campaign and over the biomass burning event, respectively. The corresponding averages of the total CCN number concentrations ($N_{CCN,S}$) and of the total CCN efficiencies ($N_{CCN,S}/N_{CN,tot}$) are summarized in Table 2. As illustrated in Fig. 7a, the average CN size distribution for the entire campaign was monomodal with a maximum at $\sim$70 nm, and the corresponding total particle number concentration was $N_{CN,tot}$=1.8×10^4 cm^{-3} (Table 2). At S=0.068% the CCN size distribution accounted only for $\sim$5% of $N_{CN,tot}$, because only a minor fraction of the CN were larger than the activation diameter ($\sim$200 nm). At S=0.27–0.87% the CCN activation diameters were close to the maximum of the CN number mode and the integral CCN efficiencies were substantially higher

(a)

(b)
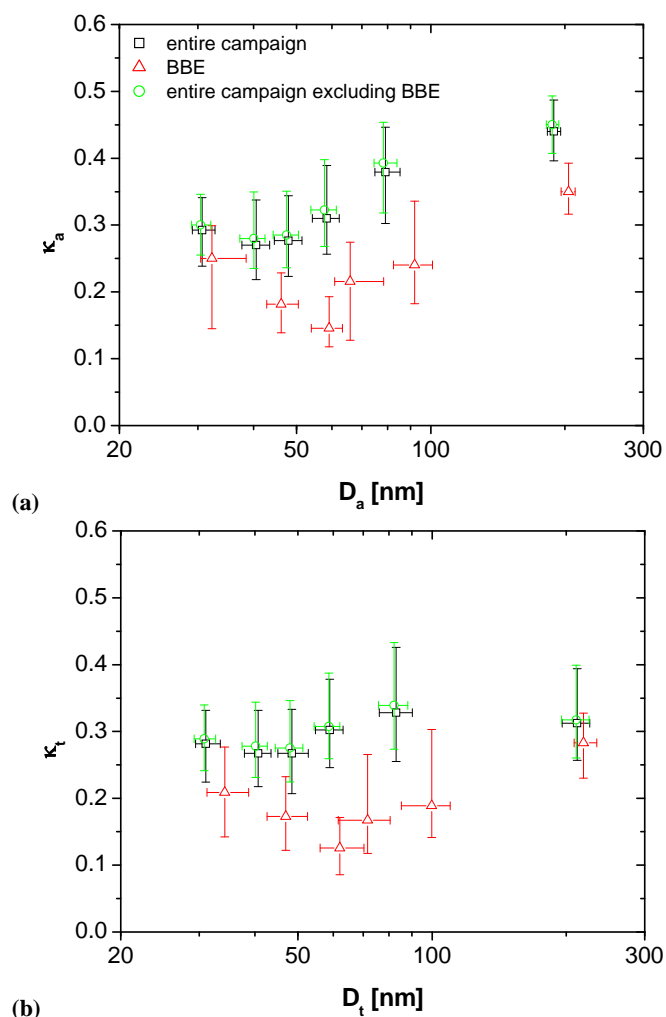
Fig. 6. Hygroscopicity parameters **(a)** for the CCN-active particles (κ_a) and **(b)** for the total aerosol (κ_t) averaged over different periods: the entire campaign, the Biomass Burning Event (BBE) and the campaign excluding the biomass burning event. The data points are median values corresponding to a given level of supersaturation, and the error bars extend to lower and upper quartiles.

($N_{CCN,S}/N_{CN,tot}$=36–71%; Table 2). During the biomass burning event (Fig. 7b), the CN size distribution was broader and the maximum was shifted to larger sizes ($\sim$120 nm, a value typical of biomass smoke; Reid et al., 2005). The average number concentration of CN was slightly smaller ($\sim$1.5×10^4 cm^{-3}), but due to the larger average particle sizes the CCN number concentrations at S=0.068% and 0.27% were higher (+90% and +8%, respectively). For $S \geq$0.47%, however, $N_{CCN,S}$ was lower compared to the rest of the campaign (Table 2).
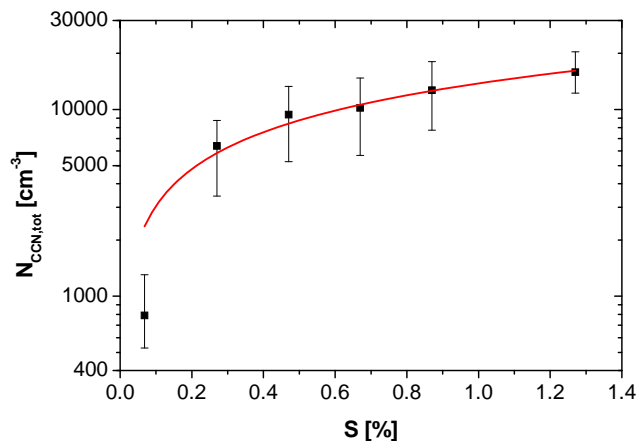
The geometric mean diameters (D_g), standard deviations (σ_g), and integral number concentrations (N_g) of monomodal lognormal fits to the median CN size distributions were D_g=70 nm, σ_g=1.94, and N_g=14 600 cm^{-3} for the entire

(a)

(b)

Fig. 8. CCN number concentrations ($N_{CCN,S}$) averaged over the entire campaign and plotted against water vapor supersaturation (S). The data points are median values, and error bars extend to lower and upper quartiles. The red line is a classical power law fit of the function $N_{CCN,S}=N_{CCN,1} \cdot (S/(1\%))^k$ with the best fit parameters $N_{CCN,1}=13\,699\,cm^{-3}$ and $k=0.65$ ($R^2=0.97$, $n=6$).

are the highest CCN number concentrations that have been measured and reported so far (Andreae, 2009; Andreae and Rosenfeld, 2008; Wiedensohler et al., 2009).

3.3 Prediction of CCN number concentration

In this section we compare different model approaches for the approximation/prediction of CCN concentration as a function of water vapor supersaturation, aerosol particle number concentration, size distribution and hygroscopicity: (1) the classical power law approach relating $N_{CCN,S}$ to $N_{CCN,1}$, i.e. to the CCN concentration at $S=1\%$; (2) a modified power law approach relating $N_{CCN,S}$ to the concentration of aerosol particles with $D>30\,nm$ ($N_{CN,30}$); and (3) the κ-Köhler model approach relating $N_{CCN,S}$ to the aerosol particle size distribution ($dN_{CN}/d\log D$) and effective hygroscopicity. For all data points obtained during the campaign, the model results were compared with the observed values, and the mean values of the relative deviations are summarized in Table 3.

3.3.1 Classical power law

Figure 8 shows the campaign median values of $N_{CCN,S}$ plotted against S and a power law fit of the function $N_{CCN,S}=N_{CCN,1} \cdot (S/(1\%))^k$ (Pruppacher and Klett, 1997; Origin 6.1G software, Levenberg-Marquardt algorithm). The obtained fit parameter $N_{CCN,1} \approx 1.4 \times 10^4\,cm^{-3}$ is substantially higher than any previously reported value, and $k \approx 0.65$ is within the range of values reported for other continental locations (0.4–0.9; Pruppacher and Klett, 1997; Andreae, 2009). The mean relative deviations of the individual measurement data points from the average power law were in the

Fig. 7. Number size distributions of total aerosol particles (CN) and Cloud Condensation Nuclei (CCN) averaged over **(a)** the entire campaign and **(b)** the biomass burning event. The CCN size distributions were calculated by multiplying the median CN size distribution with the median CCN efficiency spectra from Fig. 3. For clarity and to avoid potential biases due to different averaging times, CCN size distributions are displayed only for the supersaturation levels covered throughout the campaign.

campaign, and $D_g=107\,nm$, $\sigma_g=2.09$, and $N_g=14\,200\,cm^{-3}$ for the biomass burning event.

The number concentration of total aerosol particles ($N_{CN,tot}$) and cloud condensation nuclei ($N_{CCN,S}$) exhibited high temporal variability throughout the campaign with ranges of $\sim10^3$–$4\times10^4\,cm^{-3}$ for $N_{CN,tot}$ and $\sim10^2$–$3\times10^3\,cm^{-3}$, $\sim10^3$–$2\times10^4\,cm^{-3}$, and $\sim3\times10^3$–$3\times10^4\,cm^{-3}$ for $N_{CCN,S}$ at $S=0.068\%$, 0.27%, and 0.87%, respectively. The corresponding mean values and standard deviations are listed in Table 2. To our knowledge, these

Table 3. Characteristic deviations between observed CCN number concentrations $N_{CCN,S}$ and CCN number concentrations predicted by different model approaches ($N_{CCN,S,p}$): arithmetic mean values of the relative bias ($\Delta_b N_{CCN,S}=(N_{CCN,S,p}-N_{CCN,S})/N_{CCN,S}$) and of the total relative deviation ($\Delta_d N_{CCN,S}=|N_{CCN,S,p}-N_{CCN,S}|/N_{CCN,S}$, including systematic and statistical errors). CPL is the classical power law and MPL the modified power law approach, respectively. SD_m is the campaign average CN size distribution (Fig. 7a), and SD_u and SD_r are the generic urban and rural size distributions as listed in Seinfeld and Pandis (2006, Table 8.3), respectively. n_{SD} is the number of data points.

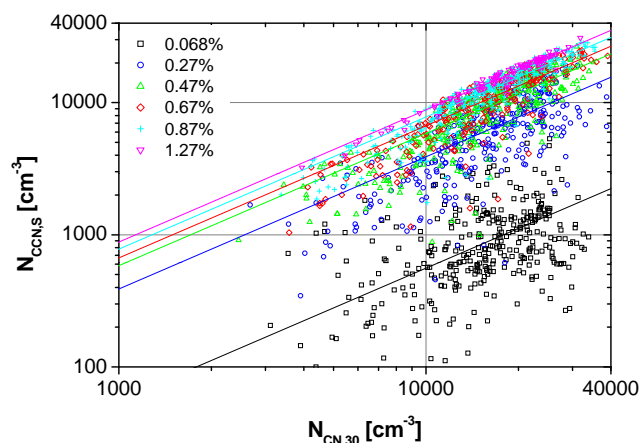| S [%]	CPL bias [%]	CPL dev. [%]	MPL bias [%]	MPL dev. [%]	κ_t var. bias [%]	κ_t var. dev. [%]	κ_a var. bias [%]	κ_a var. dev. [%]	κ_t=0.3 bias [%]	κ_t=0.3 dev. [%]	κ_a=0.34 bias [%]	κ_a=0.34 dev. [%]	κ_{cut}=0.26 bias [%]	κ_{cut}=0.26 dev. [%]	κ_t var., const. SD_m bias [%]	κ_t var., const. SD_m dev. [%]	κ_t var., const. SD_u bias [%]	κ_t var., const. SD_u dev. [%]	κ_t var., const. SD_r bias [%]	κ_t var., const. SD_r dev. [%]	n_{SD}
0.068	+310.7	313.3	+33.9	63.6	+2.5	8.6	+41.4	41.4	+4.2	19.5	+16.6	24.9	−8.8	18.8	+33.2	71.5	+95.3	113.8	−75.3	77.2	331
0.27	+54.6	89.6	+32.5	53.4	+6.7	7.4	+13.2	13.5	+6.4	17.2	+13.0	19.4	−1.0	16.5	+38.9	72.1	+123.4	132.4	−74.6	76.3	331
0.47	+37.7	75.2	+22.1	37.5	+5.1	5.8	+6.9	7.3	+8.4	12.8	+12.9	15.2	+3.3	11.4	+35.2	68.2	+134.7	138.8	−76.7	77.4	337
0.67	+57.1	85.5	+20.2	33.0	+4.3	4.6	+5.9	6.3	+11.4	14.0	+15.1	16.5	+7.2	12.0	+45.6	74.4	+171.5	173.3	−75.2	75.9	230
0.87	+41.2	69.2	+11.9	21.3	+3.4	3.6	+4.0	4.1	+7.5	9.0	+10.1	10.7	+4.6	7.6	+26.7	60.6	+161.3	162.6	−78.0	78.1	327
1.27	+23.8	43.3	+1.9	6.2	+4.7	4.7	+5.0	5.0	+5.7	6.0	+6.9	6.9	+4.3	5.4	−1.5	39.1	+145.9	145.9	−81.1	81.1	97
all	+98.3	124.1	+23.1	40.3	+4.4	6.0	+14.2	14.5	+7.2	14.0	+13.1	16.8	+0.8	12.9	+33.2	67.3	+135.6	142.4	−76.3	77.3	1653

Table 4. Fit parameter Q and q of the fit functions $N_{CCN,S}=N_{CN,30}\cdot(S/(1\%))^Q$ and $N_{CCN,S}=N_{CN,30}\cdot s^{-q}$, respectively. The correlation coefficient R^2 is the same for both fits. n_{SD} is the number of data points.

| S [%]	s	Q	q	R^2	n_{SD}
0.068	1.00068	1.07	4242	0.04	331
0.27	1.0027	0.72	349.8	0.49	331
0.47	1.0047	0.71	114.5	0.69	337
0.67	1.0067	1.01	60.29	0.78	230
0.87	1.0087	1.78	28.67	0.87	327
1.27	1.0127	−0.53	9.95	0.95	97

Fig. 9. CCN number concentrations ($N_{CCN,S}$) observed at different supersaturation levels plotted against the number concentration of aerosol particles with $D>30\,nm$ ($N_{CN,30}$). The lines are modified power law fits of the function $N_{CCN,S}=N_{CN,30}\cdot s^{-q}$ with the parameter q as given in Table 4.

range of 40–90% for S=0.27–1.27%, but as high as 310% for S=0.068% (Table 3).

3.3.2 Modified power law

Figure 9 shows all observed values of $N_{CCN,S}$ plotted against $N_{CN,30}$ and power law fits of the form $N_{CCN,S}=N_{CN,30}\cdot s^{-q}$ with $s=1+S/(100\%)$ (Pruppacher and Klett, 1997; Origin 6.1G software, Levenberg-Marquardt algorithm). An overview of the best fit values obtained for the exponent q and the corresponding correlation coefficients is given in Table 4. In this approach, CN with $D<30\,nm$ were excluded, because they are generally not CCN-active and highly variable due to new particle formation (nucleation events). Moreover, the water vapor saturation ratio s was used instead of the supersaturation S, because the exponent varies more regularly with s than with S (Table 4: monotonous dependence of q on s vs. non-monotonous dependence of Q on S). At high supersaturations ($S\geq0.47\%$), $N_{CCN,S}$ was fairly well correlated to $N_{CN,30}$ (R^2=0.69–0.95), and the mean relative deviations between the power law fit and the observed values of $N_{CCN,S}$ were less than 40%

(Table 3). At S=0.27% the correlation was much worse (R^2=0.49, mean deviation 54%), and at S=0.068% there was practically no correlation and the individual $N_{CCN,S}$ data points deviated by up to one order of magnitude from the power law fit (R^2=0.04, mean deviation 64%).

3.3.3 κ-Köhler model with variable CN size distribution

In Fig. 10, predicted CCN number concentrations ($N_{CCN,S,p}$) that were obtained with the κ-Köhler model and different hygroscopicity parameters are plotted against observed values of $N_{CCN,S}$. For each data point, $N_{CCN,S,p}$ was calculated by integrating the measured CN size distribution above the critical dry particle diameter for CCN activation that corresponds to the given values of κ and S (Sects. 2.2.4 and 3.2).

(a)

(b)
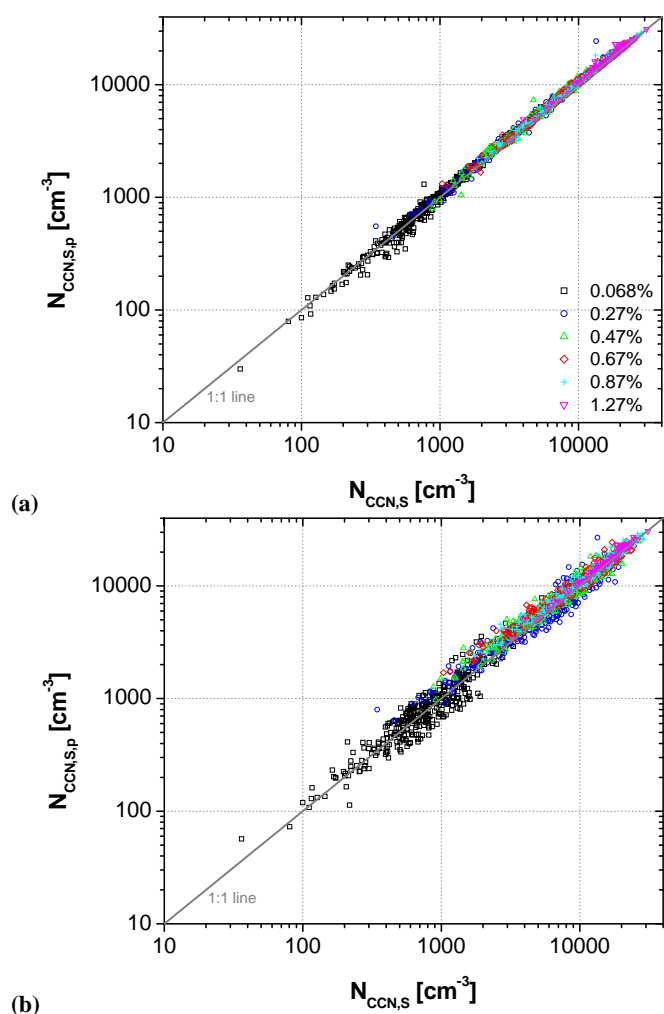
Fig. 10. Predicted CCN number concentrations ($N_{CCN,S,p}$) based on the κ-Köhler model approach **(a)** with variable values of κ_t as derived from individual CCN efficiency spectra and **(b)** with a constant average value of $\kappa=0.3$ plotted against the observed CCN number concentrations ($N_{CCN,S}$).

As illustrated in Fig. 10a, the predicted and observed values of $N_{CCN,S}$ are in very good agreement, when for each data point κ_t was taken from the CCN efficiency spectrum measured in parallel to the CN size distribution. With this approach, the mean relative deviation averaged over all supersaturations was only 6%, and the overall mean bias of the model values was +4% (Table 3). The agreement demonstrates that κ_t is a suitable proxy for the effective hygroscopicity and CCN activity of the investigated ensemble of aerosol particles including CCN-active and -inactive particles. The deviations and the bias increased with lower S, which can be explained by the decreasing MAF, indicating that the effect of external mixing between CCN-active and -inactive particles is not fully captured by κ_t. Nevertheless, the results obtained with κ_t were clearly better than with κ_a,

which represents the effective hygroscopicity of the CCN-active particles only and thus leads to higher mean deviation and bias (15%, +14%, Table 3). Only at $S=0.47$–1.27%, where MAF$_f \approx 1$ and $\kappa_a \approx \kappa_t$, were the results obtained with individual κ_a values nearly the same as with individual κ_t, and thus the overall mean bias and deviation were significantly higher (+14%, 15%, Table 3).

Fair agreement was also achieved when the campaign average value of $\kappa_t=0.30$ and the corresponding constant activation diameters for the prescribed supersaturation levels (215, 86, 59, 47, 39, and 30 nm; $S=0.068$–1.27%) were used for the calculation of $N_{CCN,S}$ from the individual measured CN size distributions. With this approach, the overall mean relative deviation was more than twice as high, but the bias was hardly higher than when individual κ_t values were used (14% and +7.2%, respectively; Table 3; Fig. 10b). Note that the campaign average value of κ_t equals the average value of hygroscopicity parameters observed or inferred for other continental locations (Andreae and Rosenfeld, 2008; Pöschl et al., 2009; and references therein) in agreement with global model simulations (Tsigaridis et al., 2006; Kreidenweis et al., 2009).

The approach using a constant average value of $\kappa=0.3$ cannot fully account for the observed temporal variations in aerosol composition and CCN properties. It yields relative deviations in the range of -40% to $+80\%$ of $N_{CCN,S}$. Under most circumstances, however, i.e. for 76% of all data points, the deviations were still less than $\pm20\%$, which appears quite reasonable for data that span more than two orders of magnitude. Even during the BBE, which was characterized by $\sim30\%$ lower hygroscopicity parameters ($\kappa_t \approx 0.2$; Sect. 3.1.2), the average deviation between predicted and observed $N_{CCN,S}$ was only 21%.

With average or individual values of κ_a, the positive bias was higher than with κ_t (6–10%, Table 3). The approach using individual values of κ_{cut} yielded the same concentrations as observed because $N_{CCN,S,p}$ was calculated from κ_{cut} in the reverse way as κ_{cut} from $N_{CCN,S}$. With a constant average value of $\kappa_{cut}=0.26$, the relative deviations were essentially the same as with constant κ_t.

3.3.4 κ-Köhler model with constant CN size distribution

To test the relative importance of aerosol particle size distribution and hygroscopicity for the variability of $N_{CCN,S}$, we performed additional Köhler model calculations in which the effective hygroscopicity parameters were allowed to vary (variable κ_t from the fitting of measured CCN efficiency spectra) while the CN size distribution was kept constant. In analogy to Gunthe et al. (2009), we used the campaign average size distribution (Fig. 7a) and a generic urban and rural size distribution as listed in Seinfeld and Pandis (2006, Table 8.3, based on Jaenicke, 1993) with three lognormal modes, respectively.

With the constant campaign average size distribution (Fig. 7a) and variable κ_t, the mean relative deviation between observed and predicted CCN concentrations ($\sim$70%) was higher by a factor of $\sim$5 than with the constant campaign average value of κ_t=0.3 and variable size distribution ($\sim$15%, Table 3). Assuming a constant generic size distribution for urban areas with variable κ_t, the mean relative deviation between observed and predicted CCN concentrations ($\sim$140%) was higher by a factor of 10 than under the assumption of an average value of κ_t=0.3 with variable size distribution (14%, Table 3). Assuming a constant generic size distribution for rural areas with variable κ_t, the mean relative deviation between observed and predicted CCN concentrations ($\sim$80%) were only a little higher than when assuming the campaign average size distributions, but lead to an under-prediction of $N_{CCN,S}$.

This demonstrates that the variability of CCN concentrations is much more strongly influenced by the variability of aerosol particle number concentration and size distribution than by the variability of aerosol composition and hygroscopicity. This applies for the temporal variations during the PRD 2006 campaign (factor of $\sim$5 between col. 11 and 17, Table 3) as well as for spatial/geographic variations between the Pearl River Delta and other urban regions (factor of 2 between col. 17 and 19, Table 3).

4 Summary and conclusions

The dry CCN activation diameters measured during PRIDE-PRD2006 at S=0.068–1.27% were in the range of 200–30 nm and the effective hygroscopicity parameters varied in the range of 0.1–0.5. The mean value of κ_t characterizing the hygroscopicity of all aerosol particles averaged over the whole campaign and investigated size range was 0.3, which equals the average value of κ observed or inferred for other continental locations (Andreae and Rosenfeld, 2008; Pöschl et al., 2009). Particles in the Aitken size range ($D\approx$30–70 nm, $\kappa_a\approx\kappa_t\approx$0.28) were on average less hygroscopic than particles in the accumulation size range ($D\approx$70–200 nm, $\kappa_t\approx$0.33, $\kappa_a\approx$0.41).

During a strong local Biomass Burning Event (BBE) the aerosol particles were generally less CCN active ($\kappa_t\approx$0.2). Due to the very intense local sources and high level of pollution, the κ values observed during the BBE can be regarded as characteristic for freshly emitted smoke from the open burning of agricultural waste.

At low S($\leq$0.27%), the maximum activated fraction remained generally well below one, which indicates substantial portions of externally mixed CCN-inactive particles with much lower hygroscopicity ($\kappa\approx$0.01) – most likely soot particles. At S=0.068%, the average MAF_f was only $\sim$0.75 with minimum values as low as $\sim$0.4, i.e. even at diameters as large as $\sim$250 nm an average of $\sim$25% up to $\sim$60% of the aerosol particles were not CCN-active. To

our knowledge such high portions of externally mixed CCN-inactive particles have not been observed before in atmospheric aerosols. Note, however, that these CCN-inactive particles contributed only around $\sim$3% to the total aerosol particle number concentration. The integral CCN efficiencies at moderate supersaturations ($N_{CCN,S}/N_{CN,tot}\approx$0.36–0.53 at S=0.27%–0.47%, Table 2) were even slightly higher than the global average value reported by Andreae (2009) ($N_{CCN,S}/N_{CN,tot}\approx$0.36 at S=0.4%).

From the measured CCN efficiency spectra and total aerosol particle (CN) size distributions, we derived CCN size distributions and total CCN number concentrations ($N_{CCN,S}$). On average, $N_{CCN,S}$ ranged from 1000 cm^{-3} at S=0.068% to 16 000 cm^{-3} at S=1.27%, representing $\sim$6% to $\sim$85% of the total aerosol particle number concentration ($N_{CN,tot}$). During the biomass burning event, the CN size distribution was broader and the maximum was shifted to larger sizes (from $\sim$70 nm to $\sim$120 nm). The average number concentration of CN was slightly smaller ($\sim$1.5×10^4 cm^{-3} vs. $\sim$1.8×10^4 cm^{-3}), but due to the larger average particle sizes the CCN concentrations at low supersaturation were substantially higher (+100% at S=0.068%, +10% at S=0.27%). For high supersaturations ($S\geq$0.47%), however, $N_{CCN,S}$ decreased by up to $\sim$25% compared to the rest of the campaign.

Based on the measurement data, we have tested different model approaches (power laws and κ-Köhler models) for the approximation/prediction of $N_{CCN,S}$ as a function of water vapor supersaturation, aerosol particle number concentration, size distribution and hygroscopicity. Depending on S and on the applied type of power law or hygroscopicity parameter, the relative deviations between observed and predicted $N_{CCN,S}$ can range from a few percent to several hundred percent. The largest deviations occurred at low S with power laws based on particle number concentration without size information. Much better predictions could be made when using measured aerosol size distributions in combination with κ-Köhler models.

With variable κ values obtained from individual CCN efficiency spectra, the relative deviations between observed and predicted $N_{CCN,S}$ were on average less than $\sim$10% and rarely exceeded 20%. These results confirm the applicability of the κ-Köhler model approach for efficient description of the CCN properties of atmospheric aerosols. Note, however, that in the case of externally mixed CCN-active and -inactive aerosol particles, the use of κ parameters derived from different types of fits to the measured CCN efficiency spectra (2- or 3-parameter CDF) can lead to substantially different results – especially at low S (increase of deviations by up to a factor of $\sim$4).

Assuming a constant average value of κ=0.3, the deviations were on average still less than $\sim$20%, which confirms that κ=0.3 may be suitable as a first-order approximation for the effective hygroscopicity and CCN activity of continental aerosols. Model calculations assuming constant particle

number concentrations and size distributions led to substantially larger deviations ($\sim$70% to $\sim$140%).

These findings confirm earlier studies suggesting that aerosol particle number and size are the major predictors for the variability of the CCN concentration in continental boundary layer air, followed by particle composition and hygroscopicity as relatively minor modulators (Gunthe et al., 2009; Pöschl et al., 2009; and references therein). Thus the influence of aerosol chemical composition and hygroscopicity appears to be less variable and less uncertain than other factors that determine the effects of aerosols on warm cloud formation in the atmosphere (e.g., particle number concentration, size distribution, sources, sinks, and meteorological conditions). Depending on the required and applicable level of detail, the information and parameterizations presented in this study should enable efficient description of the CCN activity of atmospheric aerosols in detailed process models as well as in large-scale atmospheric and climate models (Heintzenberg and Charlson, 2009).

Table A1. Notation (Frequently used symbols).

Symbol	Quantity, Unit
D	mobility equivalent particle diameter, nm
D_a	midpoint activation diameter determined by 3-parameter CDF fit, nm
D_t	midpoint activation diameter determined by 2-parameter CDF fit, nm
D_{cut}	apparent cut-off diameter of CCN activation, nm
MAF_f	maximum activated fraction determined by 3-parameter CDF fit
$N_{CCN,S}$	number concentration of cloud condensation nuclei (CCN) at supersaturation S, cm^{-3}
$N_{CCN,S,p}$	predicted CCN number concentration at supersaturation S, cm^{-3}
$N_{CCN,S}/N_{CN,tot}$	integral CCN efficiency (relative to $N_{CN,tot}$), cm^{-3}
$N_{CN,30}$	number concentration of aerosol particles (CN) with $D>30$ nm, cm^{-3}
$N_{CN,tot}$	number concentration of total aerosol particles (CN), cm^{-3}
S	water vapor supersaturation, %
κ	effective hygroscopicity parameter
κ_a	effective hygroscopicity parameter determined by 3-parameter CDF fit (characteristic for CCN-active particles)
κ_t	effective hygroscopicity parameter determined by 2-parameter CDF fit (proxy for overall population of aerosol particles)
κ_{cut}	effective hygroscopicity parameter determined by integration of the CN size distribution (characteristic for CCN-active particles $>D_{cut}$)

References

Andreae, M. O.: Correlation between cloud condensation nuclei concentration and aerosol optical thickness in remote and polluted regions, Atmos. Chem. Phys., 9, 543–556, 2009, http://www.atmos-chem-phys.net/9/543/2009/.

Andreae, M. O. and Rosenfeld, D.: Aerosol-cloud-precipitation interactions. Part 1, The nature and sources of cloud-active aerosols, Earth Sci. Rev., 89, 13–41, 2008.

Andreae, M. O., Schmid, O., Yang, H., Yu, J., Zeng, L., and Zhang, Y.: Optical properties and chemical composition of the atmospheric aerosol in urban Guangzhou, China, Atmos. Environ., 42, 6335–6350, doi:10.1016/j.atmosenv.2008.01.030, 2008.

Bougiatioti, A., Fountoukis, C., Kalivitis, N., Pandis, S. N., Nenes, A., and Mihalopoulos, N.: Cloud condensation nuclei measurements in the marine boundary layer of the Eastern Mediterranean: CCN closure and droplet growth kinetics, Atmos. Chem. Phys., 9, 7053–7066, 2009, http://www.atmos-chem-phys.net/9/7053/2009/.

Broekhuizen, K., Chang, R.Y.-W., Leaitch, W. R., Li, S.-M., and Abbatt, J. P. D.: Closure between measured and modeled cloud condensation nuclei (CCN) using size-resolved aerosol compositions in downtown Toronto, Atmos. Chem. Phys., 6, 2513–2524, 2006, http://www.atmos-chem-phys.net/6/2513/2006/.

Chang, R. Y.-W., Slowik, J. G., Shantz, N. C., Vlasenko, A., Liggio, J., Sjostedt, S. J., Leaitch, W. R., and Abbatt, J. P. D.: The hygroscopicity parameter (κ) of ambient organic aerosol at a field site subject to biogenic and anthropogenic influences: Relationship to degree of aerosol oxidation, Atmos. Chem. Phys. Discuss., 9, 25323–25360, 2009, http://www.atmos-chem-phys-discuss.net/9/25323/2009/.

Cheng, Y. F., Berghof, M., Garland, R. M., Wiedensohler, A., Wehner, B., Müller, T., Su, H., Zhang, Y. H., Achtert, P., Nowak, A., Pöschl, U., Zhu, T., Hu, M., and Zeng, L. M.: Influence of soot mixing state on aerosol light absorption and single scattering albedo during air mass aging at a polluted regional site in northeastern China, J. Geophys. Res., 114, D00G10, doi:10.1029/2008JD010883, 2009.

Deng, X., Tie, X., Wu, D., Zhou, X., Bi, X., Tan, H., Li, F., and Jiang, C.: Long-term trend of visibility and its characterizations in the Pearl River Delta (PRD) region, China, Atmos. Environ., 42, 1424–1435, 2008.

Dusek, U., Frank, G. P., Hildebrandt, L., Curtius, J., Schneider, J., Walter, S., Chand, D., Drewnick, F., Hings, S., Jung, D., Borrmann, S., and Andreae, M. O.: Size matters more than chemistry for cloud nucleating ability of aerosol particles, Science, 312, 1375–1378, 2006.

Dusek, U., Frank, G. P., Curtius, J., Drewnick, F., Schneider, J., Kürten, A., Rose, D., Andreae, M. O., Borrmann, S., and Pöschl, U.: Enhanced organic mass fraction and decreased hygroscopicity of cloud condensation nuclei (CCN) during new particle formation events, Geophys. Res. Lett., 37, L03804, doi:10.1029/2009GL040930, 2010.

Ervens, B., Cubison, M. J., Andrews, E., Feingold, G., Ogren, J. A., Jimenez, J. L., Quinn, P. K., Bates, T. S., Wang, J., Zhang, Q., Coe, H., Flynn, M., and Allan, J. D.: CCN predictions using simplified assumptions of organic aerosol composition and mixing state: a synthesis from six different locations, Atmos. Chem. Phys. Discuss., 9, 21237–21256, 2009, http://www.atmos-chem-phys-discuss.net/9/21237/2009/.

Fan, S., Wang, B., Tesche, M., Engelmann, R., Althausen, A., Liu, J., Zhu, W., Fan, Q., Li, M.-H., Ta, N., Song, L., and Leong, K.: Meteorological conditions and structures of atmospheric boundary layer in October 2004 over Pearl River Delta area, Atmos. Environ., 42, 6174–6186, 2008.

Frank, G. P., Dusek, U., and Andreae, M. O.: Technical note: A method for measuring size-resolved CCN in the atmosphere, Atmos. Chem. Phys. Discuss., 6, 4879–4895, 2006, http://www.atmos-chem-phys-discuss.net/6/4879/2006/.

Garland, R. M., Yang, H., Schmid, O., Rose, D., Nowak, A., Achtert, P., Wiedensohler, A., Takegawa, N., Kita, K., Miyazaki, Y., Kondo, Y., Hu, M., Shao, M., Zeng, L. M., Zhang, Y. H., Andreae, M. O., and Pöschl, U.: Aerosol optical properties in a rural environment near the mega-city Guangzhou, China: implications for regional air pollution, radiative forcing and remote sensing, Atmos. Chem. Phys., 8, 5161–5186, 2008, http://www.atmos-chem-phys.net/8/5161/2008/.

Garland, R. M., Schmid, O., Nowak, A., Achtert, P., Wiedensohler, A., Gunthe, S. S., Takegawa, N., Kita, K., Kondo, Y., Hu, M., Shao, M., Zeng, L. M., Zhu, T., Andreae, M. O., and Pöschl, U.: Aerosol optical properties observed during Campaign of Air Quality Research in Beijing 2006 (CAREBeijing-2006): Characteristic differences between the inflow and outflow of Beijing city air, J. Geophys. Res., 114, D00G04, doi:10.1029/2008JD010780, 2009.

Gunthe, S. S., King, S. M., Rose, D., Chen, Q., Roldin, P., Farmer, D. K., Jimenez, J. L., Artaxo, P., Andreae, M. O., Martin, S. T., and Pöschl, U.: Cloud condensation nuclei in pristine tropical rainforest air of Amazonia: size-resolved measurements and modeling of atmospheric aerosol composition and CCN activity, Atmos. Chem. Phys., 9, 7551–7575, 2009, http://www.atmos-chem-phys.net/9/7551/2009/.

Hagler, G. S., Bergin, M. H., Salmon, L. G., Yu, J. Z., Wan, E. C. H., Zheng, M., Zeng, L. M., Kiang, C. S., Zhang, Y. H., Lau, A. K. H., and Schauer, J. J.: Source areas and chemical composition of fine particulate matter in the Pearl River Delta region of China, Atmos. Environ., 40, 3802–3815, 2006.

Heintzenberg, J. and Charlson, R. J.: Clouds in the Perturbed Climate System - Their Relationship to Energy Balance, Atmospheric Dynamics, and Precipitation, MIT Press, Cambridge, 2009.

Hua, W., Chen, Z. M., Jie, C. Y., Kondo, Y., Hofzumahaus, A., Takegawa, N., Chang, C. C., Lu, K. D., Miyazaki, Y., Kita, K., Wang, H. L., Zhang, Y. H., and Hu, M.: Atmospheric hydrogen peroxide and organic hydroperoxides during PRIDE-PRD'06, China: their concentration, formation mechanism and contribution to secondary aerosols, Atmos. Chem. Phys., 8, 6755–6773, 2008, http://www.atmos-chem-phys.net/8/6755/2008/.

Huang, Y., Chameides, W. L., and Dickinson, R. E.: Direct and indirect effects of anthropogenic aerosols on regional precipitation over east Asia, J. Geophys. Res., 112, D03212, doi:10.1029/2006JD007114, 2007.

IAPSAG: WMO/IUGG International Aerosol Precipitation Science Assessment Group (IAPSAG) Report: Aerosol Pollution Impact on Precipitation: A Scientific Review, World Meteorological Organization, Geneva, 482, 2007.

IPCC: Climate Change 2007: The Physical Science Basis, Contribution of Working Group I to the Fourth Assessment Report of the Intergovernmental Panel on Climate Change, edited by: Solomon, S., Qin, D., Manning, M., Chen, Z., Marquis, M., Averyt, K., Tignor, M., and Miller, H. L., Cambridge University Press, Cambridge and New York, 996, 2007.

Jaenicke, R.: Aerosol cloud climate interaction, Tropospheric aerosols, edited by: Hobbs, P. V., Academic Press, San Diego, CA, 1–31, 1993.

Kreidenweis, S. M., Petters, M. D., and Chuang, P. Y.: Cloud particle precursors, Clouds in the Perturbed Climate System: Their Relationship to Energy Balance, Atmospheric Dynamics, and Precipitation, Strüngmann Forum Report, vol. 2, edited by: Heintzenberg, J. and Charlson, R. J., The MIT Press, Cambridge, MA, 2009.

Kreidenweis, S. M., Petters, M. D., and DeMott, P. J.: Single-parameter estimates of aerosol water content, Environ. Res. Lett., 3, 035002, doi:10.1088/1748-9326/3/3/035002, 2008.

Kuwata, M., Kondo, Y., Mochida, M., Takegawa, N., and Kawamura, K.: Dependence of CCN activity of less volatile particles on the amount of coating observed in Tokyo, J. Geophys. Res.-Atmos., 112, D11207, doi:10.1029/2006JD007758, 2007.

Kuwata, M., Kondo, Y., Miyazaki, Y., Komazaki, Y., Kim, J. H., Yum, S. S., Tanimoto, H., and Matsueda, H.: Cloud condensation nuclei activity at Jeju Island, Korea in spring 2005, Atmos. Chem. Phys., 8, 2933–2948, 2008, http://www.atmos-chem-phys.net/8/2933/2008/.

Kuwata, M., Kondo, Y., and Takegawa, N.: Critical condensed mass for activation of black carbon as cloud condensation nuclei in Tokyo, J. Geophys. Res., 114, D20202, doi:10.1029/2009JD012086, 2009.

Lance, S., Medina, J., Smith, J. N., and Nenes, A.: Mapping the Operation of the DMT Continuous Flow CCN Counter, Aerosol Sci. Tech., 40, 242–254, 2006.

Lance, S., Nenes, A., Mazzoleni, C., Dubey, M. K., Gates, H., Varutbangkul, V., Rissman, T. A., Murphy, S. M., Sorooshian, A., Flagan, R. C., Seinfeld, J. H., Feingold, G., and Jonsson, H. H.: Cloud condensation nuclei activity, closure, and droplet growth kinetics of Houston aerosol during the Gulf of Mexico Atmospheric Composition and Climate Study (GoMACCS), J. Geophys. Res., 114, D00F15, doi:10.1029/2008JD011699, 2009.

Li, Z. Q., Xia, X., Cribb, M., Mi, W., Holben, B., Wang, P., Chen, H., Tsay, S. C., Eck, T. F., Zhao, F., Dutton, E. G., and Dickerson, R. E.: Aerosol optical properties and their radiative effects in northern China, J. Geophys. Res., 112, D22S01, doi:10.1029/2006JD007382, 2007.

Liu, B. H., Xu, M., Henderson, M., Qi, Y., and Li, Y. Q.: Taking China's temperature: Daily range, warming trends, and regional variations, 1955–2000, J. Climate, 17, 4453–4462, 2004.

Liu, X. G., Cheng, Y. F., Zhang, Y. H., Jung, J. S., Sugimoto, N., Chang, S. Y., Kim, Y. J., Fan, S. J., and Zeng, L. M.: Influences of relative humidity and particle chemical composition on aerosol scattering properties during the 2006 PRD campaign, Atmos. Environ., 42, 1525–1536, 2008.

Massie, S. T., Torres, O., and Smith, S. J.: Total Ozone Mapping Spectrometer (TOMS) observations of increases in Asian aerosol in winter from 1979 to 2000, J. Geophys. Res.-Atmos., 109, D18211, doi:10.1029/2004JD004620, 2004.

Matsumoto, K., Tanaka, H., Nagao, I., and Ishizaka, Y.: Contribution of particulate sulfate and organic carbon to cloud condensation nuclei in the marine atmosphere, Geophys. Res. Lett., 24, 655–658, 1997.

McFiggans, G., Artaxo, P., Baltensperger, U., Coe, H., Facchini, M. C., Feingold, G., Fuzzi, S., Gysel, M., Laaksonen, A., Lohmann, U., Mentel, T. F., Murphy, D. M., O'Dowd, C. D., Snider, J. R., and Weingartner, E.: The effect of physical and chemical aerosol properties on warm cloud droplet activation, Atmos. Chem. Phys., 6, 2593–2649, 2006,
http://www.atmos-chem-phys.net/6/2593/2006/.

Mikhailov, E., Vlasenko, S., Martin, S. T., Koop, T., and Pöschl, U.: Amorphous and crystalline aerosol particles interacting with water vapor: conceptual framework and experimental evidence for restructuring, phase transitions and kinetic limitations, Atmos. Chem. Phys., 9, 9491–9522, 2009,
http://www.atmos-chem-phys.net/9/9491/2009/.

Niedermeier, D., Wex, H., Voigtländer, J., Stratmann, F., Brüggemann, E., Kiselev, A., Henk, H., and Heintzenberg, J.: LACIS-measurements and parameterization of sea-salt particle hygroscopic growth and activation, Atmos. Chem. Phys., 8, 579–590, 2008,
http://www.atmos-chem-phys.net/8/579/2008/.

Petters, M. D. and Kreidenweis, S. M.: A single parameter representation of hygroscopic growth and cloud condensation nucleus activity, Atmos. Chem. Phys., 7, 1961–1971, 2007,
http://www.atmos-chem-phys.net/7/1961/2007/.

Petters, M. D., Carrico, C. M., Kreidenweis, S. M., Prenni, A. J., DeMott, P. J., Collett Jr., J. L., and Moosmüller, H.: Cloud condensation nucleation activity of biomass burning aerosol, J. Geophys. Res., 114, D22205, doi:10.1029/2009JD012353, 2009.

Pöschl, U., Rose, D., and Andreae, M. O.: Climatologies of Cloud-related Aerosols: Part 2: Particle Hygroscopicity and Cloud Condensation Nuclei Activity, Clouds in the Perturbed Climate System: Their Relationship to Energy Balance, Atmospheric Dynamics, and Precipitation, Strüngmann Forum Report, vol. 2, edited by: Heintzenberg, J. and Charlson, R. J., The MIT Press, Cambridge, MA, 2009.

Pruppacher, H. R. and Klett, J. D.: Microphysics of clouds and precipitation, Kluwer Academic Publishers, Dordrecht, 288–289, 1997.

Qian, Y., Kaiser, D. P., Leung, L. R., and Xu, M.: More frequent cloud-free sky and less surface solar radiation in China from 1955 to 2000, Geophys. Res. Lett., 33, L01812, doi:10.1029/2005GL024586, 2006.

Reid, J. S., Koppmann, R., Eck, T. F., and Eleuterio, D. P.: A review of biomass burning emissions part II: intensive physical properties of biomass burning particles, Atmos. Chem. Phys., 5, 799–825, 2005,
http://www.atmos-chem-phys.net/5/799/2005/.

Reutter, P., Su, H., Trentmann, J., Simmel, M., Rose, D., Gunthe, S. S., Wernli, H., Andreae, M. O., and Pöschl, U.: Aerosol- and updraft-limited regimes of cloud droplet formation: influence of particle number, size and hygroscopicity on the activation of cloud condensation nuclei (CCN), Atmos. Chem. Phys., 9, 7067–7080, 2009,
http://www.atmos-chem-phys.net/9/7067/2009/.

Richter, A., Burrows, J. P., Nuss, H., Granier, C., and Niemeier, U.: Increase in tropospheric nitrogen dioxide over China observed from space, Nature, 437, 129–132, 2005.

Rissler, J., Vestin, A., Swietlicki, E., Fisch, G., Zhou, J., Artaxo, P., and Andreae, M. O.: Size distribution and hygroscopic properties of aerosol particles from dry-season biomass burning in Amazonia, Atmos. Chem. Phys., 6, 471–491, 2006,
http://www.atmos-chem-phys.net/6/471/2006/.

Roberts, G. C., Andreae, M. O., Zhou, J., and Artaxo, P.: Cloud condensation nuclei in the Amazon Basin: "marine" conditions over a continent?, Geophys. Res. Lett., 28(14), 2807–2810, 2001.

Roberts, G. C., Artaxo, P., Jingchuan, Z., Swietlicki, E., and Andreae, M. O.: Sensitivity of CCN spectra on chemical and physical properties of aerosol: a case study from the Amazon Basin, J. Geophys. Res., 107(D20), LBA37-1-18, 2002.

Roberts, G. C., Nenes, A., Seinfeld, J. H., and Andreae, M. O.: Impact of biomass burning on cloud properties in the Amazon Basin, J. Geophys. Res.-Atmos., 108(D2), 4062, doi:10.1029/2001JD000985, 2003.

Roberts, G. C. and Nenes, A.: A Continuous-Flow Streamwise Thermal-Gradient CCN Chamber for Atmospheric Measurements, Aerosol Sci. Tech., 39, 206–221, 2005.

Roberts, G., Mauger, G., Hadley, O., and Ramanathan, V.: North American and Asian aerosols over the eastern Pacific Ocean and their role in regulating cloud condensation nuclei, J. Geophys. Res., 111, D13205, doi:10.1029/2005JD006661, 2006.

Rose, D., Gunthe, S. S., Mikhailov, E., Frank, G. P., Dusek, U., Andreae, M. O., and Pöschl, U.: Calibration and measurement uncertainties of a continuous-flow cloud condensation nuclei counter (DMT-CCNC): CCN activation of ammonium sulfate and sodium chloride aerosol particles in theory and experiment, Atmos. Chem. Phys., 8, 1153–1179, 2008,
http://www.atmos-chem-phys.net/8/1153/2008/.

Rose, D., Garland, R. M., Yang, H., Gunthe, S. S., Berghof, M., Wehner, B., Wiedensohler, A., Takegawa, N., Kondo, Y., Andreae, M. O., and Pöschl, U.: Cloud condensation nuclei in polluted air and biomass burning smoke near the mega-city Guangzhou, China – Part 2: Size-resolved aerosol chemical composition, diurnal cycles, and mixing state of CCN-inactive soot particles, Atmos. Chem. Phys. Discuss., in preparation, 2010a.

Rose, D., Nowak, A., Achtert, P., Wiedensohler, A., Hu, M., Shao, M., Zhang, Y., Andreae, M. O., and Pöschl, U.: Interactive comment on "Cloud condensation nuclei in polluted air and biomass burning smoke near the mega-city Guangzhou, China – Part 1: Size-resolved measurements and implications for the modeling of aerosol particle hygroscopicity and CCN activity" by D. Rose et al., Atmos. Chem. Phys. Discuss., S12611, 2010b.

Rosenfeld, D., Dai, J., Yu, X., Yao, Z., Xu, X., Yang, X., and Du, C.: Inverse relations between amounts of air pollution and orographic precipitation, Science, 315, 1396–1398, 2007.

Rosenfeld, D., Lohmann, U., Raga, G. B., O'Dowd, C. D., Kulmala, M., Fuzzi, S., Reissell, A., and Andreae, M. O.: Flood or Drought: How Do Aerosols Affect Precipitation?, Science, 321, 1309–1313, 2008.

Segal, Y. and Khain, A.: Dependence of droplet concentration on aerosol conditions in different cloud types: Application to droplet concentration parameterization of aerosol conditions, J. Geophys. Rev., 111, D15204, doi:10.1029/2005JD006561, 2006.

Seinfeld, J. H. and Pandis, S. N.: Atmospheric chemistry and physics, from air pollution to climate change, John Wiley and Sons, 2006.

Shantz, N. C., Chang, R. Y.-W., Slowik, J. G., Vlasenko, A., Abbatt, J. P. D., and Leaitch, W. R.: Slower CCN growth kinetics of anthropogenic aerosol compared to biogenic aerosol observed at a rural site, Atmos. Chem. Phys., 10, 299-312, 2010, http://www.atmos-chem-phys.net/10/299/2010/.

Shao, M., Tang, X., Zhang, Y., and Li, W.: City clusters in China: air and surface water pollution, Front. Ecol. Environ., 4, 353–361, 2006.

Streets, D. G., Tsai, N. Y., Akimoto, H., and Oka, K.: Sulfur dioxide emissions in Asia in the period 1985–1997, Atmos. Environ., 34, 4413–4424, 2000.

Streets, D. G., Yu, C., Wu, Y., Chin, M., Zhao, Z., Hayasaka, T., and Shi, G.: Aerosol trends over China, 1980–2000, Atmos. Res., 88, 174–182, 2008.

Wang, J., Lee, Y.-N., Daum, P. H., Jayne, J., and Alexander, M. L.: Effects of aerosol organics on cloud condensation nucleus (CCN) concentration and first indirect aerosol effect, Atmos. Chem. Phys., 8, 6325–6339, 2008, http://www.atmos-chem-phys.net/8/6325/2008/.

Wang, X., Carmichael, G., Chen, D., Tang, Y., and Wang, T.: Impacts of different emission sources on air quality during March 2001 in the Pearl River Delta (PRD) region, Atmos. Environ., 39, 5227–5241, 2005.

Wehner, B., Berghof, M., Cheng, Y. F., Achtert, P., Birmili, W., Nowak, A., Wiedensohler, A., Garland, R. M., Pöschl, U., Hu, M., and Zhu, T.: Mixing state of nonvolatile aerosol particle fractions and comparison with light absorption in the polluted Beijing region, J. Geophys. Res., 114, D00G17, doi:10.1029/2008JD010923, 2009.

Wendisch, M., Hellmuth, O., Ansmann, A., Heintzenberg, J., Engelmann, R., Althausen, D., Eichler, H., Müller, D., Hu, M., Zhang, Y., and Mao, J.: Radiative and dynamic effects of absorbing aerosol particles over the Pearl River Delta, China, Atmos. Environ., 42, 6405–6416, 2008.

Wiedensohler, A., Cheng, Y. F., Nowak, A., Wehner, B., Achtert, P., Berghof, M., Birmili, W., Wu, Z. J., Hu, M., Zhu, T., Takegawa, N., Kita, K., Kondo, Y., Lou, S. R., Hofzumahaus, A., Holland, F., Wahner, A., Gunthe, S. S., Rose, D., Su, H., and Pöschl, U.: Rapid aerosol particle growth and increase of cloud condensation nucleus activity by secondary aerosol formation and condensation: A case study for regional air pollution in northeastern China, J. Geophys. Res.–Atmos., 114, doi:10.1029/2008JD010884, 2009.

Xu, Q.: Abrupt change of the mid-summer climate in central east China by the influence of atmospheric pollution, Atmos. Environ., 35, 5029–5040, 2001.

Yum, S. S., Hudson, J. G., Song, K. Y., and Choi, B. C.: Springtime cloud condensation nuclei concentrations on the west coast of Korea, Geophys. Res. Lett., 32, L09814, doi:10.1029/2005GL022641, 2005.

Yum, S. S., Roberts, G., Kim, J. H., Song, K. Y., and Kim, D. Y.: Submicron aerosol size distributions and cloud condensation nuclei concentrations measured at Gosan, Korea, during the Atmospheric brown clouds East Asian Regional Experiment 2005, J. Geophys. Res., 112, D22S32, doi:10.1029/2006JD008212, 2007.

Zhang, Y. H., Hu, M., Zhong, L. J., Wiedensohler, A., Liu, S. C., Andreae, M. O., Wang, W., and Fan, S. J.: Regional Integrated Experiments on Air Quality over Pearl River Delta 2004 (PRIDE-PRD2004): Overview, Atmos. Environ., 42, 6157–6173, doi:10.1016/j.atmosenv.2008.03.025, 2008.

Zhang, Y. L., Qin, B. Q., and Chen, W. M.: Analysis of 40 year records of solar radiation data in Shanghai, Nanjing and Hangzhou in Eastern China, Theor. Appl. Climatol., 78, 217–227, 2004.

Zhao, C., Tie, X., and Lin, Y.: A possible positive feedback of reduction of precipitation and increase in aerosols over eastern central China, Geophys. Res. Lett., 33, L11814, doi:10.1029/2006GL025959, 2006.